



AMS 92nd Annual Meeting

Development of an Advanced Technique for Mapping and Monitoring Sea and Lake Ice in Preparation for GOES-R Advanced Baseline Imager (ABI)

By

Rouzbeh Nazari

Date: 01/26/2012

Time: 1:45 PM

Presentation Overview

Research Importance, Objectives and Hypothesis

Sea Ice Mapping Evolution

Study Area and Data Acquisition
Data Preprocessing and Analysis

Model Development
Multiple Regression Analysis
Neural Network
Threshold Base Mapping Model

Results Comparison
Projection of Developed Tools

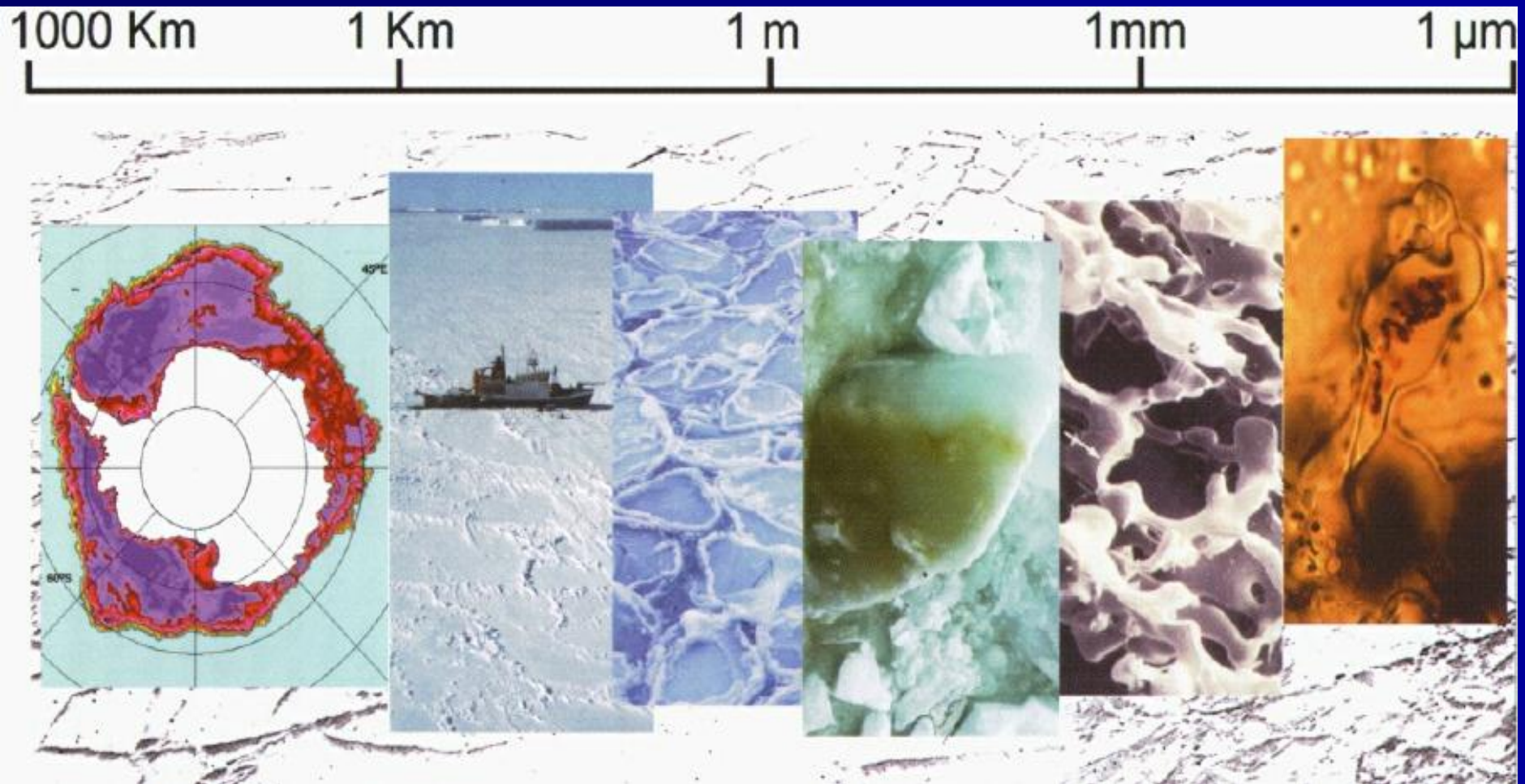
Conclusions

Sea Ice Importance

In recent years, the uniqueness of the Earth's ice-affected regions and their importance to the world is being increasingly recognized. They are considered vital and valuable for a variety of reasons:

- **Marine Transport** – Marine trade is a vital part of world economies, and it is increasing. Sea ice is a serious obstacle in the North, and icebergs affect marine transport even in temperate waters.
- **Weather and Climate Change** – As a key component of the world's weather and climate system, knowledge of current and changing ice conditions is critical to the prediction of weather and climate events.
- **Natural Resources** – Ice-affected regions are rich in resources such as oil and gas, minerals, timber, and fish, but their production is often impeded by ice.
- **Environment** – Ice-affected ecosystems are adapted to, and depend upon, ice. They are increasingly under threat from climate change, resource exploitation, marine traffic, and human habitation.
- **Habitation** – The North is home to an increasing population that must cope with a hostile icescape and adapt to changing environmental conditions.

Studies on Sea Ice



The ultimate objective of this research is to explore the potentials of the future GOES-R ABI in mapping sea ice and to develop an automated ice-mapping algorithm, which would make maximum use of ABI's improved observing capabilities.

This technique will be designed and adapted for the future GOES-R.

Data from the European Meteosat Second Generation (MSG) SEVIRI instrument, which serves as the prototype, will be used in the development and validation of this technique.

This research aims to generate the following products:

- Hourly Ice Map
- Daily Ice Map with Cloud
- Daily Cloud-free ice map (multi-date image composited approach)

Similar to snow, the reflectance of thick ice cover is very high in the visible and drops substantially in the shortwave- and middle-infrared. This specific spectral signature provides the physical basis for ice identification from space. It will be primarily used in the new ice detection algorithm for GOES-R ABI.

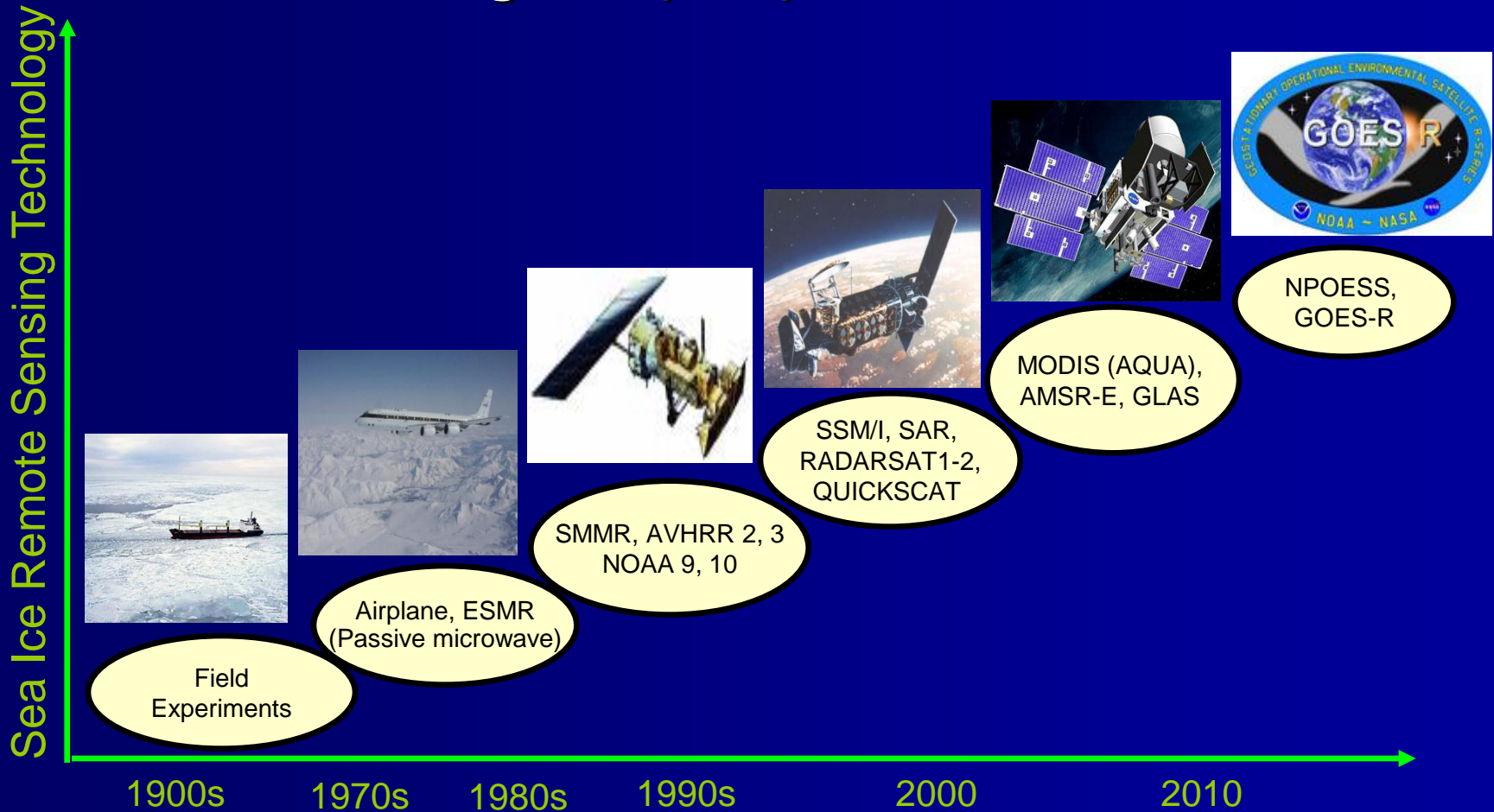
Clouds present the major factor hampering ice identification and mapping.

Ice has lower temperature than water.

As compared to polar orbiting satellite data, availability of frequent observations from geostationary satellites increases the chance to obtain a cloud clear view during a day and thus helps to reduce cloud gaps in the ice map.

Sea Ice Remote Sensing Evolution

Common wavelength VIS, NIR, Passive and Active Microwave



Data Acquisition and Study Area

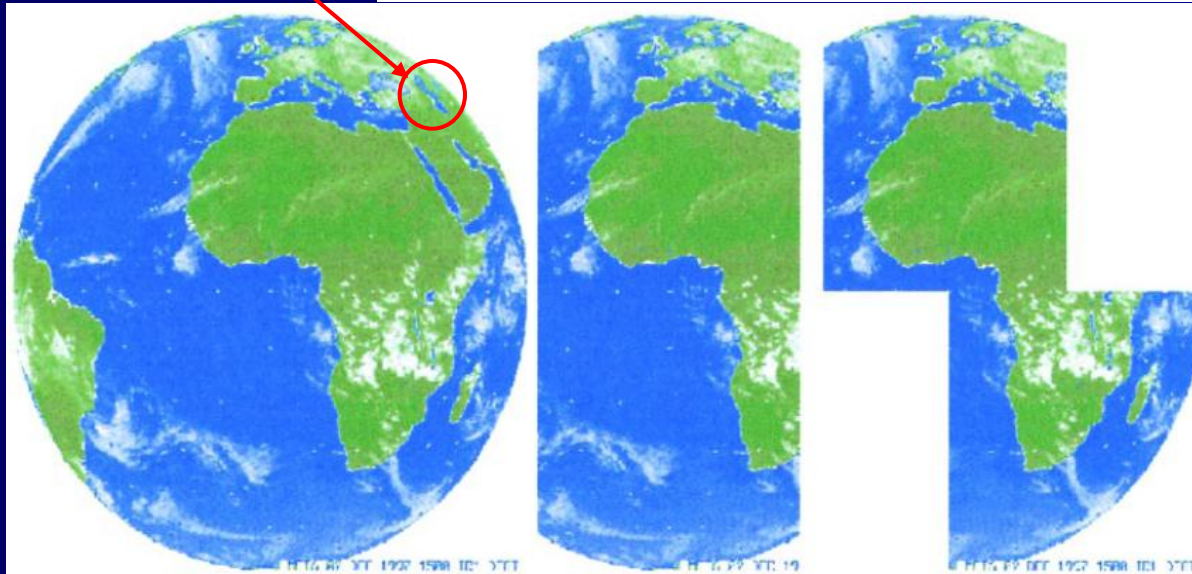
Meteosat Second Generation (MSG), SEVIRI

The Meteosat Second Generation (MSG) mission is the continuous observation of the earth's full disk. This is achieved with the Spinning Enhanced Visible and Infrared Imager (SEVIRI) imaging radiometer. SEVIRI is a 12-channel imager observing the earth-atmosphere system. Eleven channels observe the earth's full disk with a 15-min repeat cycle.

The MSG SEVIRI Instrument Radiometric Performance Characteristics

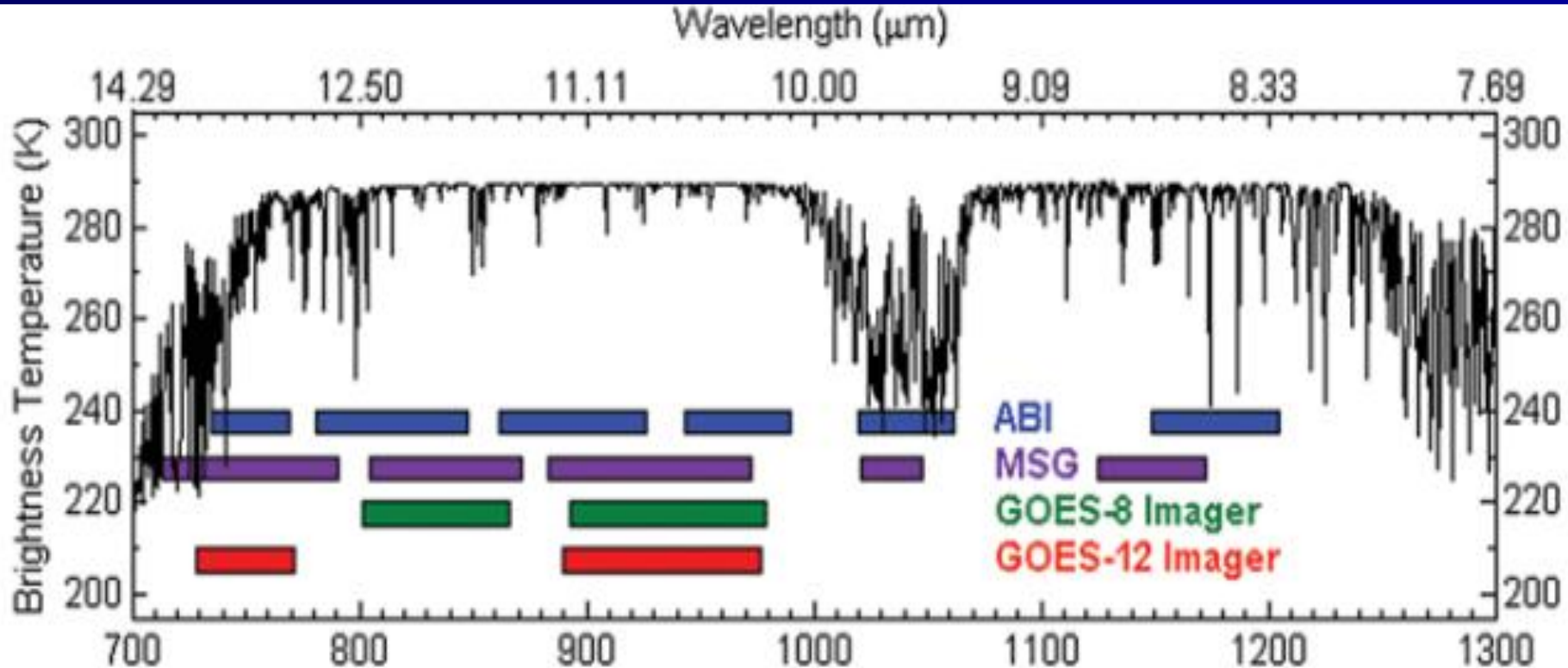
Channel (μm)	HRV	0.6	0.8	1.6	3.9	6.2	7.3	8.7	9.7	10.8	12.0	13.4
Noise	0.52	0.39	0.36	0.08	0.24	0.40	0.48	0.15	0.24	0.13	0.21	0.29
Spec.	1.07	0.53	0.49	0.25	0.35	0.75	0.75	0.28	1.50	0.25	0.37	1.80

Caspian Sea



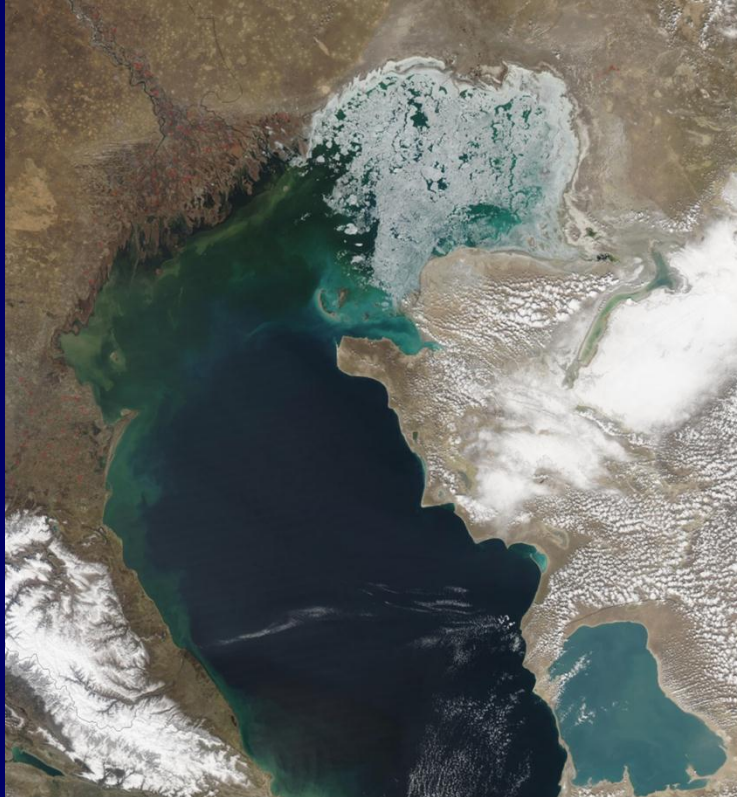
Coverage with SEVIRI on MSG, in its nominal position at 0° lon, for a repeat cycle of 15 min for channels 1–11. The full disk image has 3712×3712 pixels. The HRV (right) covers only half of the earth in the E–W direction with 11136×5568 pixels; however, the area of imaging can be selected. Scanning of SEVIRI is from east to west and south to north.

GEOS-R ABI vs. MSG SEVIRI

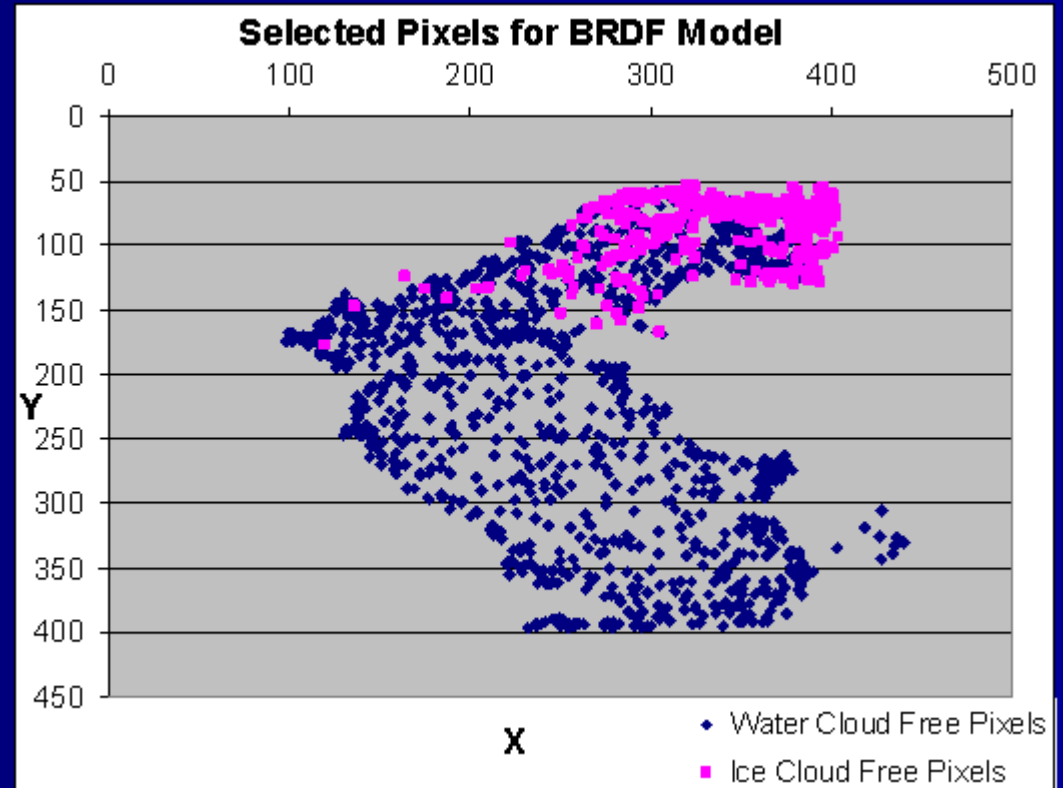


Spectral coverage of 10 ABI bands in the infrared region superimposed on a calculation of Earth-emitted spectral brightness temperatures for the U.S. Standard Atmosphere. The spectral coverage of the GOES-8 and -12 imagers, along with that of the Meteosat Second Generation (MSG, referred to as Meteosat-8) are also shown.

Selected Pixels for BRDF Model



Caspian Sea March 31, 2003
Aqua/MODIS Land Rapid Response Team



Classification Approach

METEOSAT imagery over Caspian Sea at 30 minutes interval has been routinely collected since December 2006. The following spectral bands are collected:

Reflectances:

- High resolution visible (HRV: 0.6 - 0.9 μm)
- Visible (0.6 μm),
- Visible (0.8 μm)
- Shortwave infrared (1.6 μm)

Brightness temperatures:

- Middle infrared (3.9 μm)
 - Infrared (10.8 μm)
 - Infrared (12.0 μm)
- Land/water mask will be applied. Only pixels covered with water will be considered.

Truth data:

- Results of our visual analysis of satellite imagery.
- NOAA Interactive snow and ice maps generated within IMS system.
- Other interactive ice products if available (e.g. ice maps from the Russian Hydrometeorological Service)

An image compositing procedure will be applied to reduce the cloud amount in the daily ice map. Minimum reflectance and maximum temperature compositing approach will be tested.

Ice and clear water will be distinguished from clouds using both spectral criteria and temporal variability of the scene reflectance and temperature during a day.

Night brightness temperature will be used to reduce the number of cloudy pixels.

Correction of satellite-observed reflectance for atmospheric effects and sea surface reflectance anisotropy using:

- look-up tables constructed through direct radiative transfer calculations
- 6S (Second Simulation of the Satellite Signal in the Solar Spectrum)
- Kernel-driven BRDF models with empirically-derived kernel loads.

The effect of variable water properties (e.g., higher reflectance due to sediments, river deltaic deposits, shallow water, etc.) will be assessed.

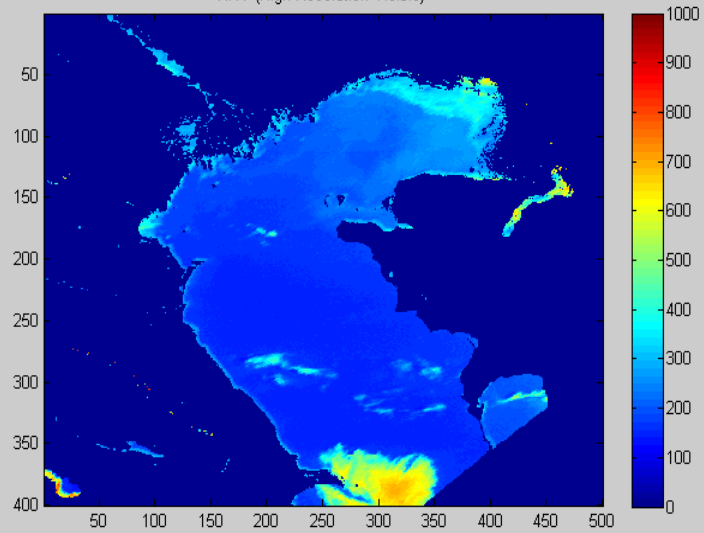
If a pixel remains unclassified after all these tests, it will be either tagged as cloudy pixel or assumed to have the class of the previous day (water/ice). Quality control flags for the pixels classified with the multi-date approach will be provided based on the number of days used to make decision.

Two final products will be produced daily:

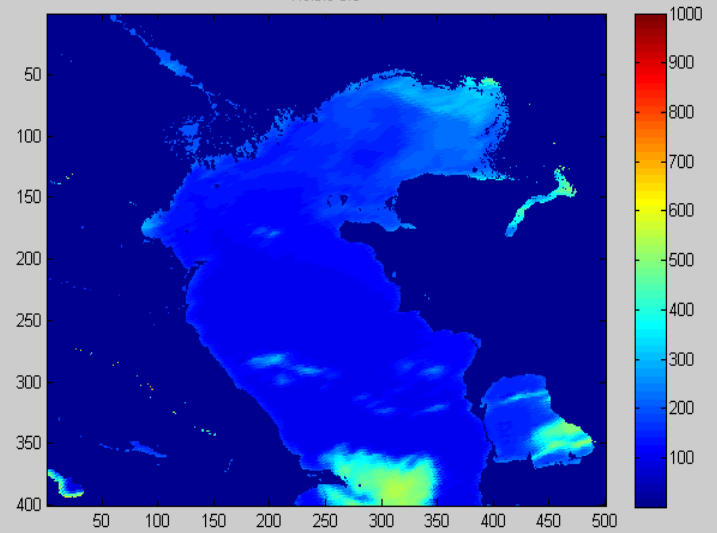
- Ice map with unclassified (or cloudy) pixels
- Cloud-free ice maps (multi-date approach).

January 23, 2007 : 11:45 local time, Channels (Reflectance)

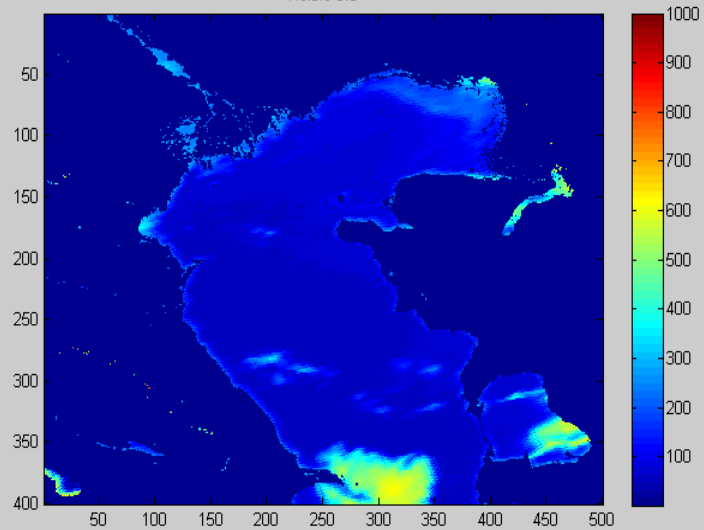
HRV (High Resolution Visible)



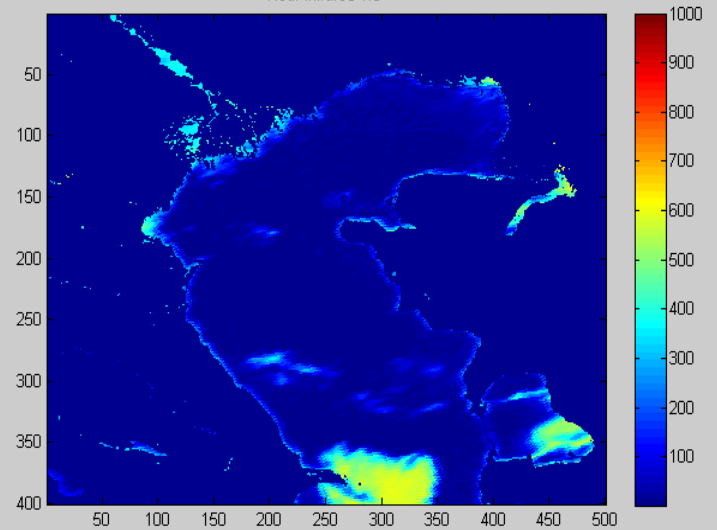
Visible 0.6



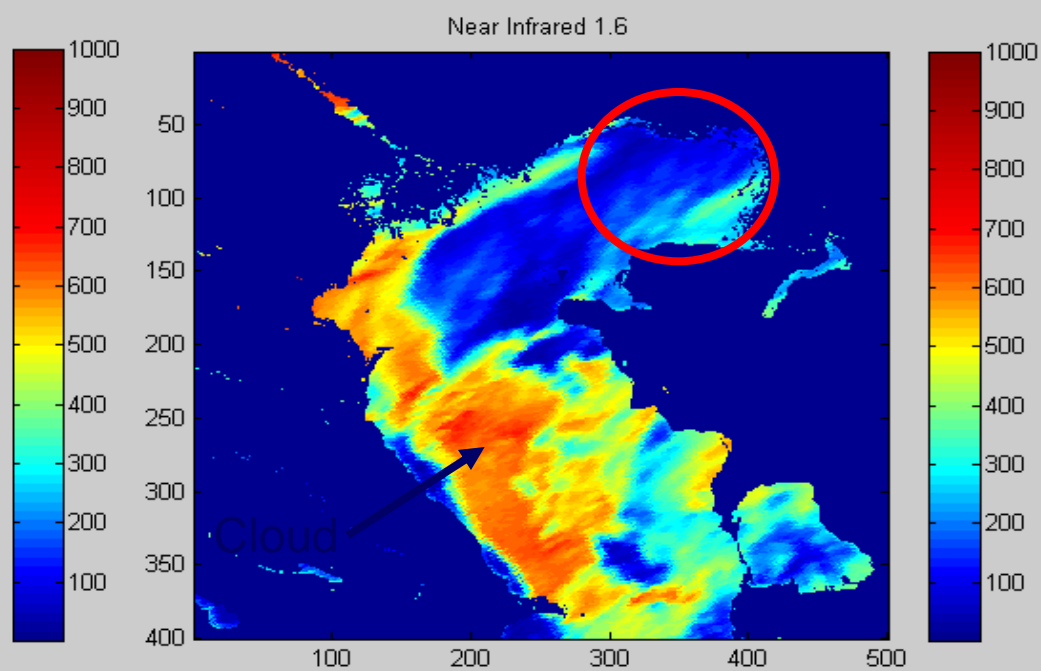
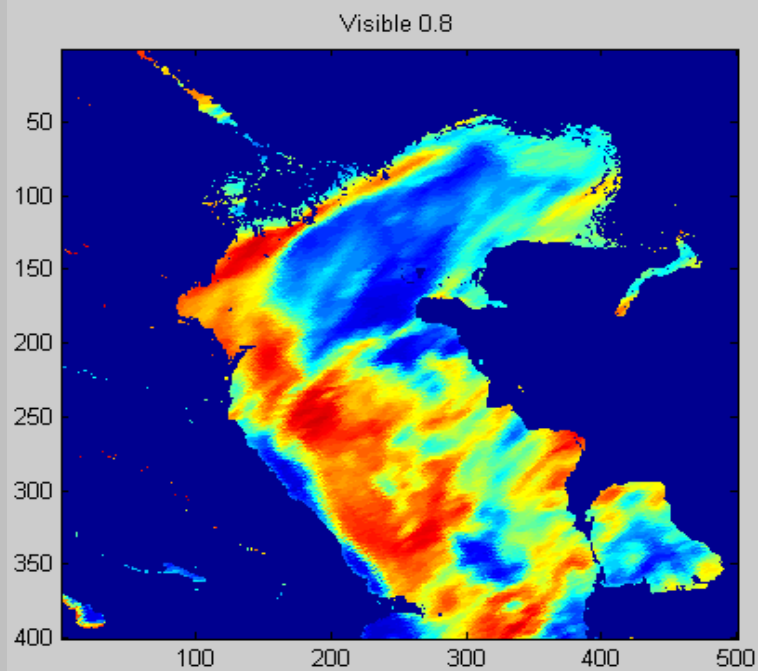
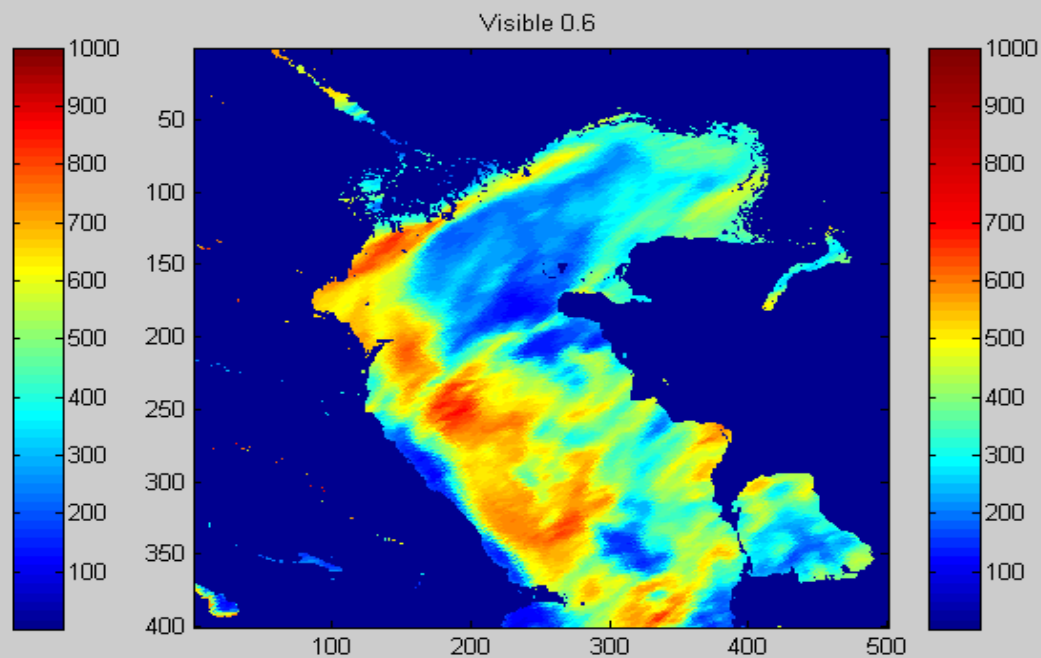
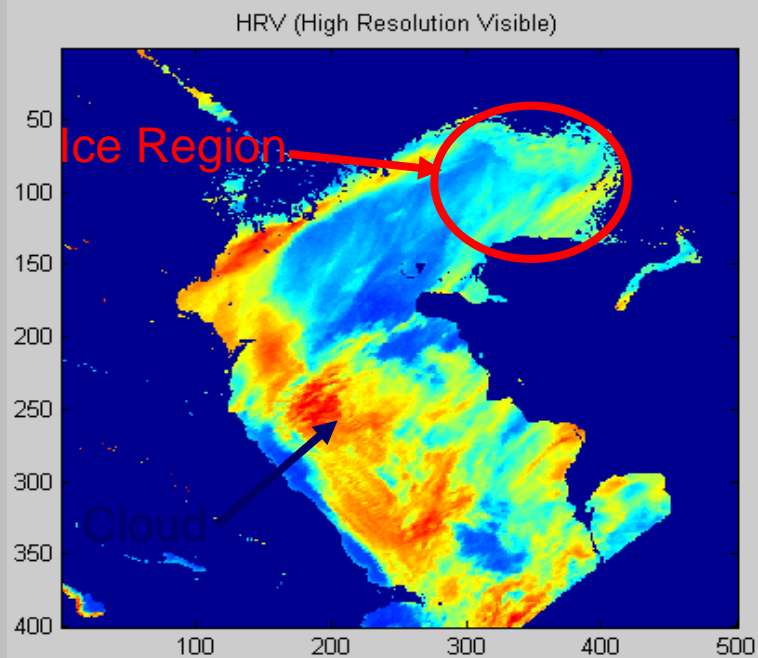
Visible 0.8



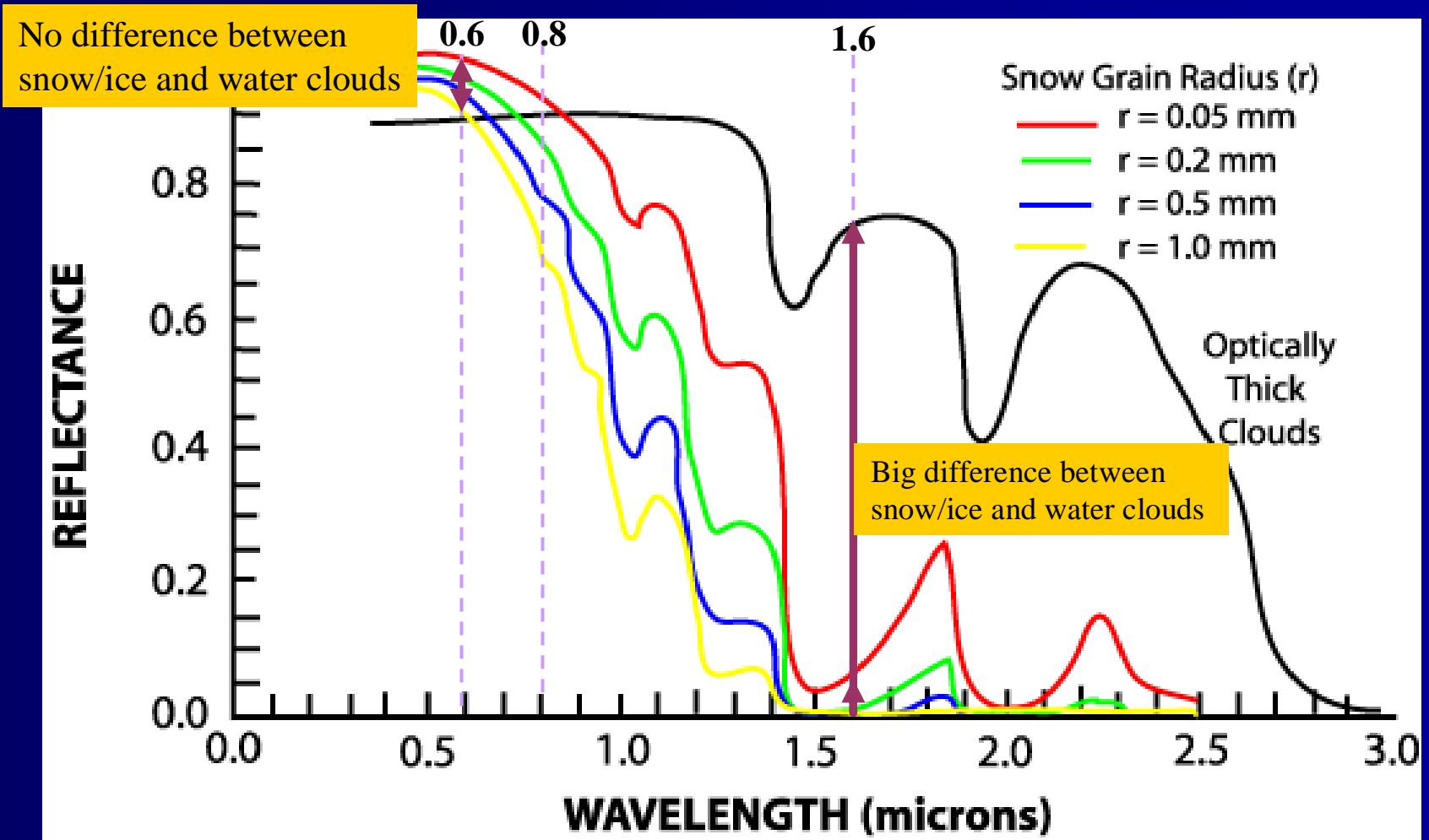
Near Infrared 1.6



February 3, 2007 : 10:45 local time, Channels (Reflectance)

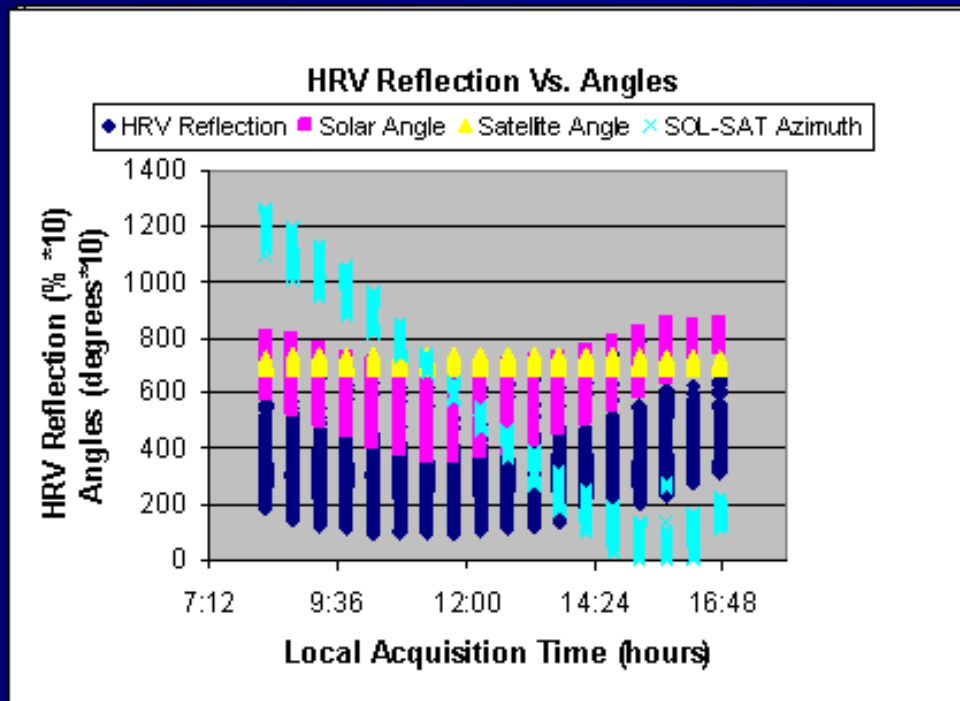


Different Reflectivity of Ice/snow and Watercloud in 1.6 μ

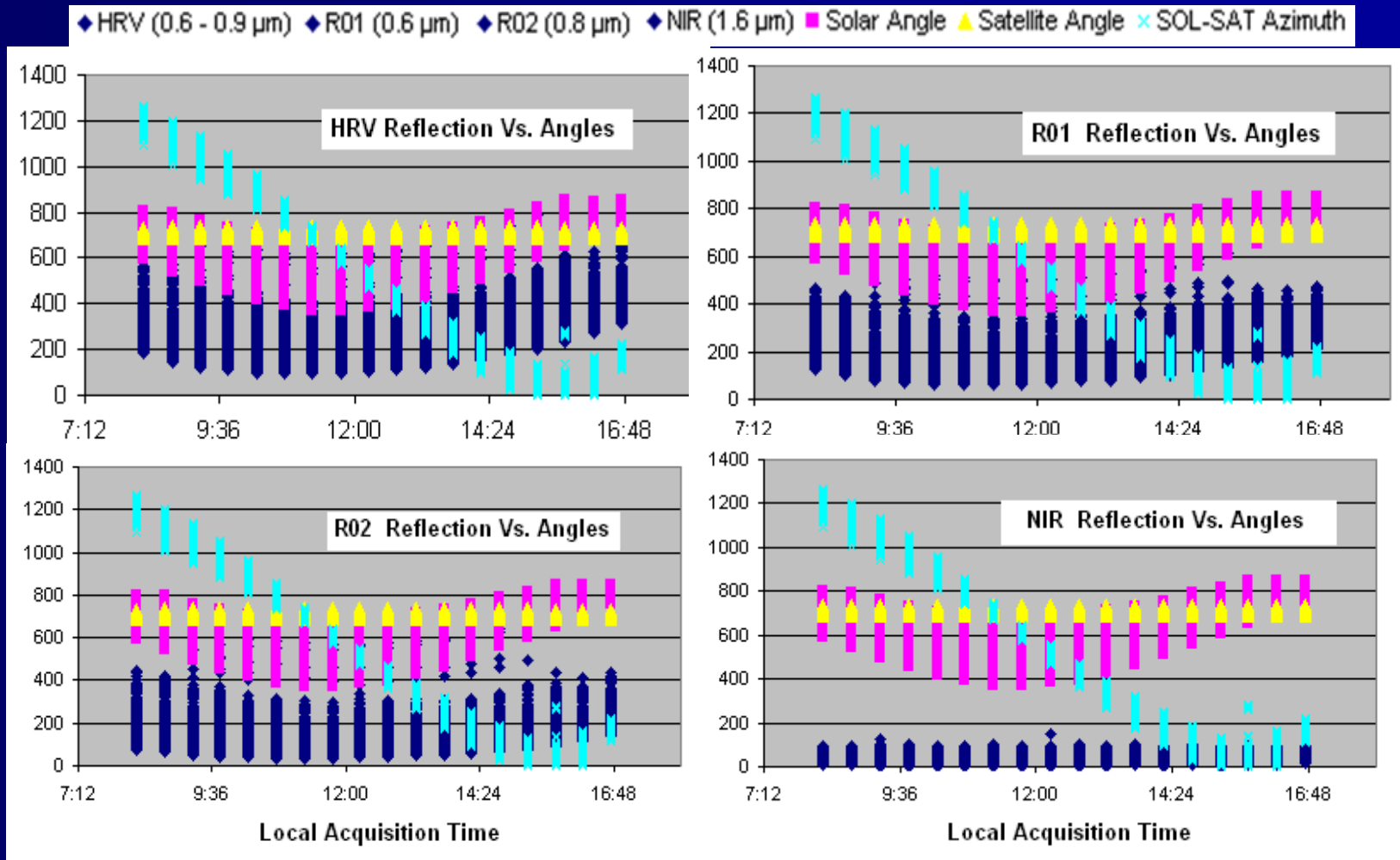


After source: EUMETSAT

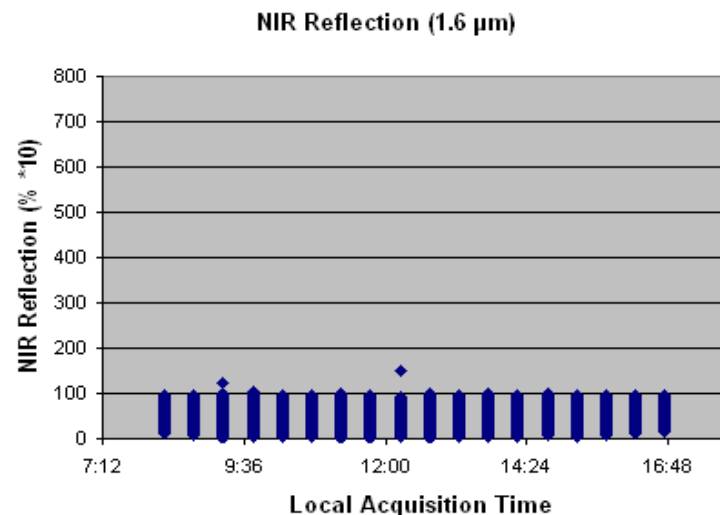
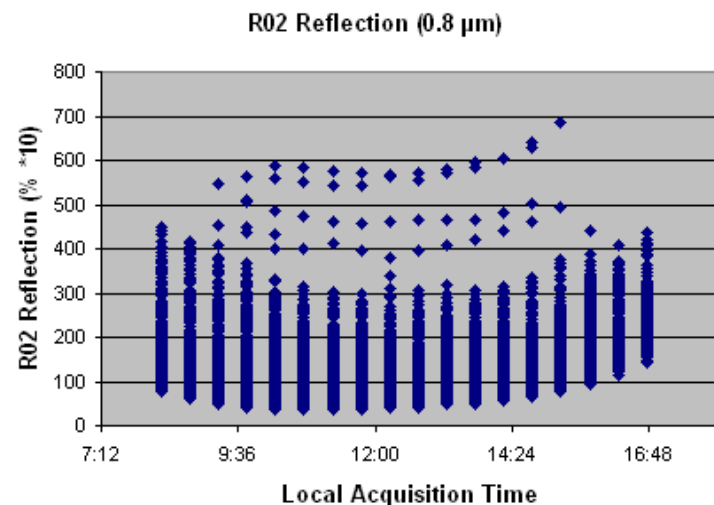
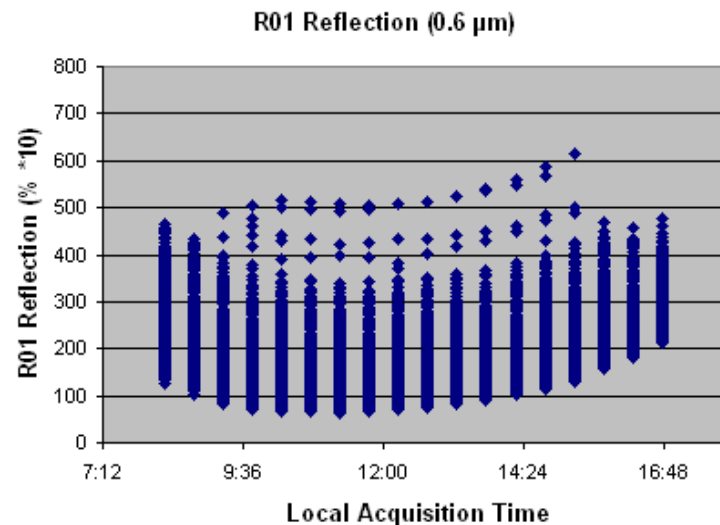
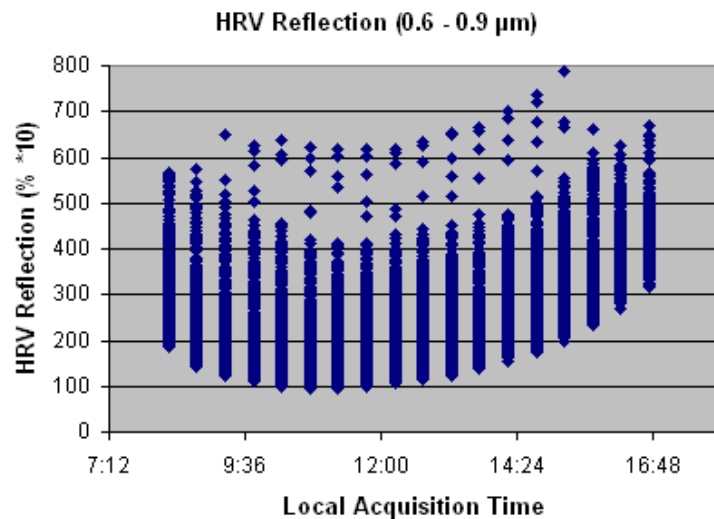
HRV Reflection (0.6-0.9 μm) Vs. Satellite Angles



Effect of Sun Irradiance and Sensor Viewing Angles on the Reflected Radiance



Daily Reflection Variation Range Distribution



Daily Angular Variation Range Distribution

Solar Irradiance Angle

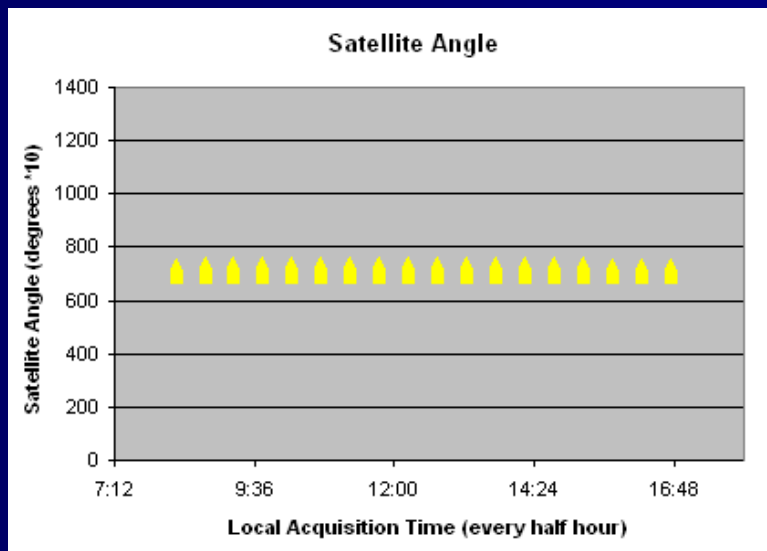
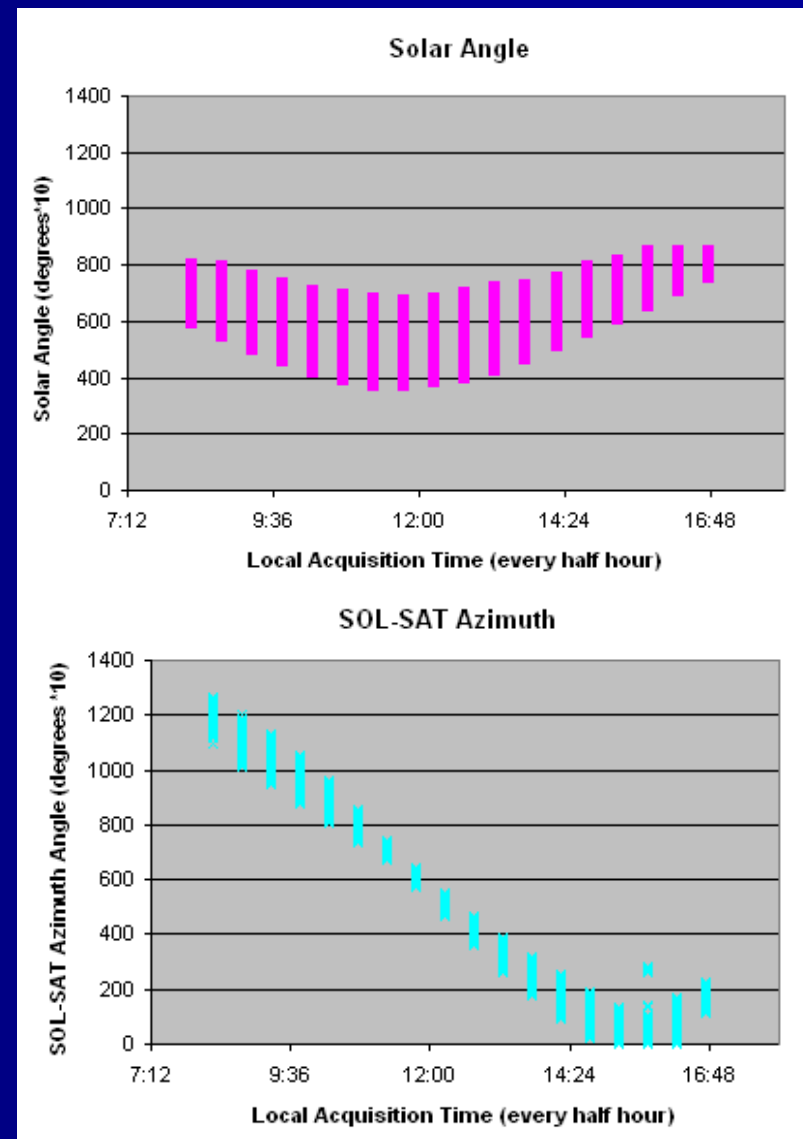
- Minimum – 12 pm of local time
- Maximum – Sun rise and sun set

Satellite Viewing Angle

= constant for specific pixel (GEOS)

SOL-SAT Azimuth Angle

- Minimum when Sun and Satellite in the same position



Angular Variation Range Distribution During Acquisition Period of Dec – March

Solar Irradiance Angle

Minimum Range – December

Maximum Range – March

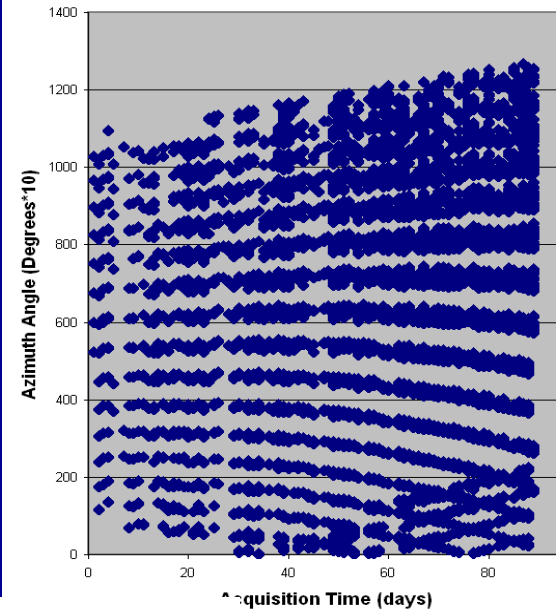
Satellite Viewing Angle

constant for specific pixel (GEOS), Less cloud free pixels in December and January

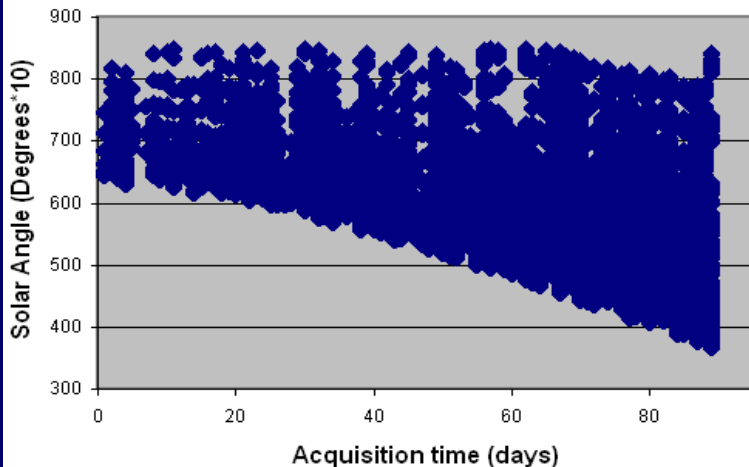
SOL-SAT Azimuth Angle

Range of Azimuth Angle grows with longer days

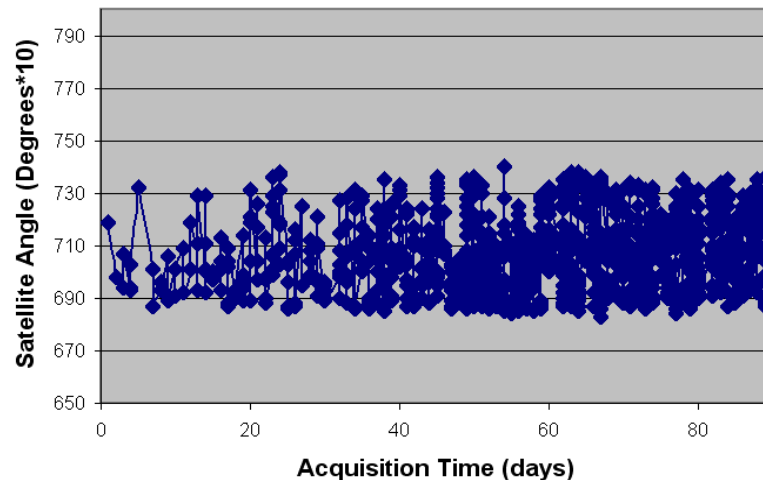
SOL-SAT Azimuth Ranges



Solar Angle Ranges



Satellite Angle Ranges



Stepwise Multiple Linear Regression

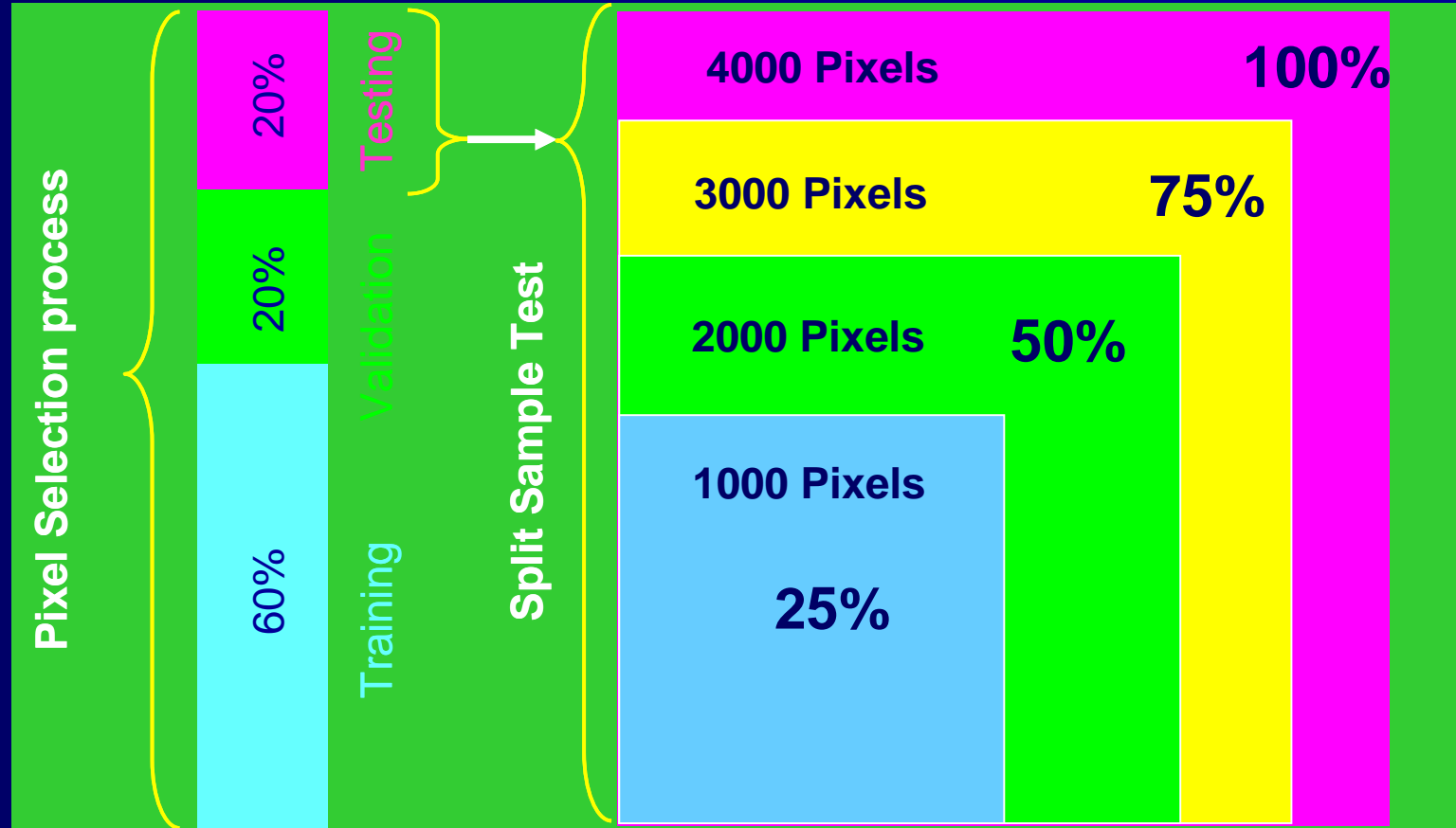
- Remote sensing has applied several statistical methods to estimate a relationship of the most significant predictors to one or more predictables in order to improve phenomenon observation and achieve considerably accurate information.
- Compared to unvaried techniques (narrow band indices and red edge inflection point) multivariate regression such as Stepwise Multiple Linear Regression (SMLR), improves the estimation of different characteristics.
- Stepwise multiple regression was used to relate spectral reflectance (the response variable to be explained, z) with viewing angle geometry (explanatory variables, X_j ($j = 1, \dots, k$)) by the following model:

$$z = b_0 + b_1 X_1 + b_2 X_2 + \dots + b_k X_k$$

- Where b_j is a coefficient to be estimated ($j = 0, 1, 2, \dots, k$). When the data are acquired by remote sensing instruments, considering the experimental error e_j , not the value corresponding to z , but an estimate y_j is obtained:

$$y_j = z + e_j$$

Pixel Selection and Validation and Testing process



Sample of selected coefficients (bj) of the variables (Xj) for the reflectance models

Set	B ^a	C ^b	D ^c	Cos B	Cos C	Cos D	Sin B	Sin C	Sin D	1/CosB	1/CosC	1/Cos D	
RV-1	4071.44	0	59557.66	3593.02	81039.14	38416.11	-1414.41	0	-5436.97	0	0	0	
RV-2	3114.09	12580993	0	2823.13	10945638	19048.18	-1056.49	0	0	0	0	9.41	
RV-3	1819.51	12925051	23816.74	0	11232847	30688.29	0	0	0	0	0	9131.83	
RV-4	-339.18	61906845	0	2232.47	53688659	141509	-790.92	0	0	0	0	0	
RV-5	-24494.9	-1.2E+09	-144551	3443.57	-1E+09	-33153.7	-1298.11	0	-10603.1	0	0	0	
RV-6	2393.51	9714654	-234750	2671.11	8746670	97613.75	-820.50	0	-20520.9	0	0	0	
RV-7	5894.94	-5091239	-267728	5062.12	-3931639	101381.6	-3484.21	0	-20849.3	0	0	0	
RV-8	2573.59	195423.3	-245670	3018.73	530922.7	101816.2	-956.62	0	-21121	0	0	0	
Sin B	1/Sin C	1/Sin D	B*C	B*D	C*D	B/C	B/D	C/D	C/B	D/B	D/C	1/B	
0	0	0	0	-2084.04	0	0	-444.27	2943.14	0	0	-45392.6	0	
0	0	15989.7	0	-1630.39	4410.19	0	0	-10335.5	0	0	15854.37	0	
0	0	21642.85	0	-1240.78	0	0	246.57	-6671.38	0	0	6262.07	0	
0	0	0	0	0	68664.99	0	0	6692.76	-2.03	2.15	19534.24	0	
0	0	0	13323.44	-1894.22	67171.8	15797.63	-281.57	0	0	0	48280.56	0	
0	0	-34106.6	0	-1622.02	203611.3	0	0	32387.48	0	0	60719.19	0	
32.92	0	-34845.7	0	-1750	221777.2	0	-104.8	33034.02	0	-0.73	74545.31	1833.81	
0	0	-34713.9	0	-1588.7	211885.3	0	0	33200.58	0	0	65002.15	0	
1/C	1/D	B/ CosB	B/ CosC	B/ Cos D	C/ Cos B	C/ CosC	C/ CosD	D/ CosB	D/ CosC	D/ CosD	CosB * CosC	CosB * CosD	CosC * CosD
0	0	0	354.92	25.69	0	0	0	0	1782.62	0	-4096.9	2214.95	-48327.34
3406224.47	0	0	297.65	0	0	0	0	0	0	0	-2675.05	2736.74	0
3519910.24	0	0	0	-17.31	0	0	0	0	0	0	0	2186.34	0
3369755.36	0	0	376.59	0	0	0	0	0	0	0	-4276.97	0	-56477.79
01834917.1	0	0	0	12.38	0	0	0	0	0	0	-3817.66	2226.8	-39508.40
2650639.39	0	0	366.25	0	0	0	0	0	0	0	-4332.81	2294.06	-159227.03
0	0	0	338.02	0	0	0	0	0	0	0	-3926.07	2330.42	-169914.43

Statistical results of the Stepwise Multiple Linear Regression calibration for 0.6μm channel

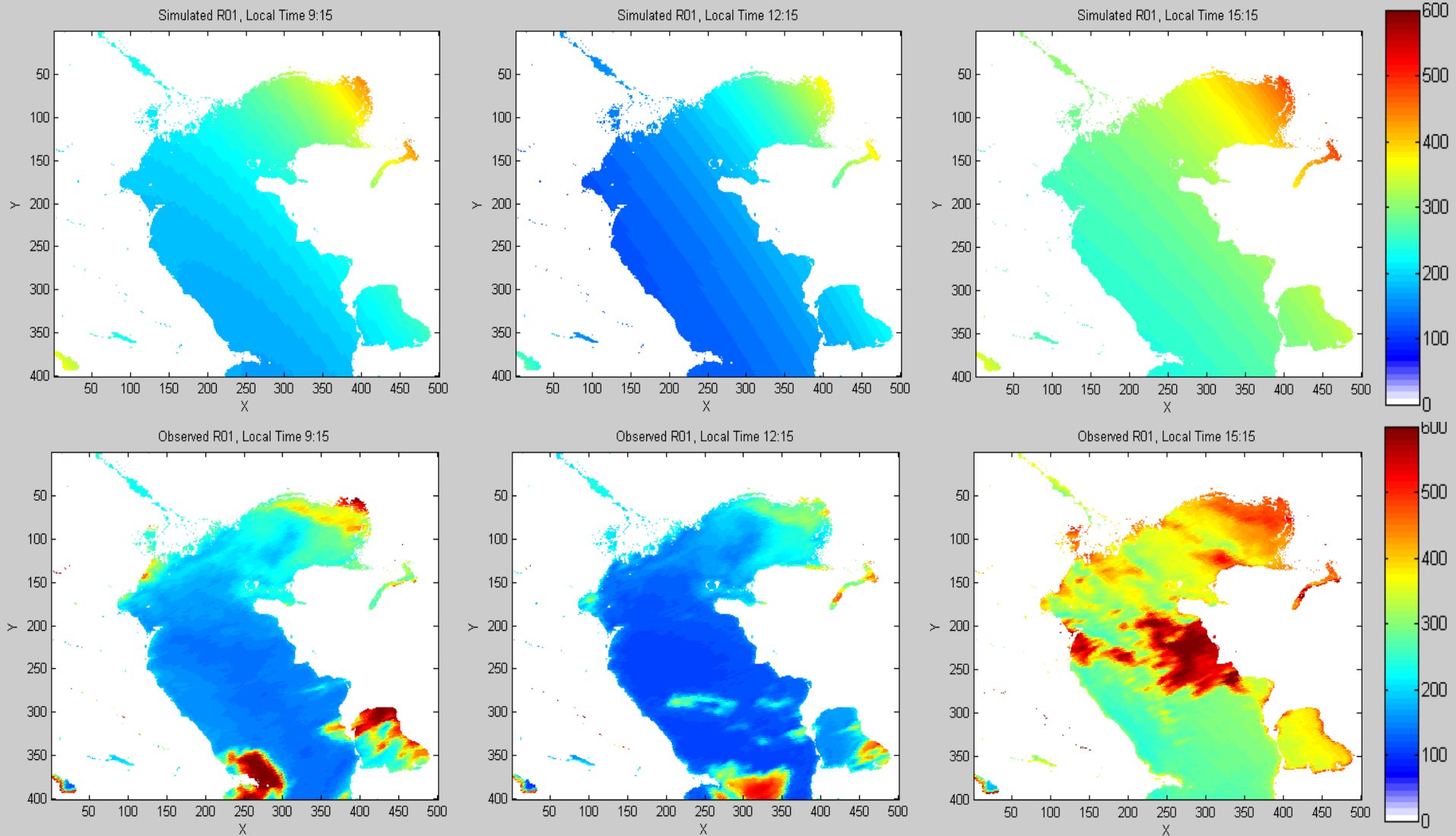
Set	Training Size	Train. Range	Test Size ^a (th)	Test Range (th)	Train. RMSE	Test RMSE (th)	Train. R ²	Test R ² (th)
R01-1	3000	2-3001	1000	4002-5001	4.07649	13.62153	0.7030	-2.1124
R01-2	3000	3002-6001	1000	1002-2001	4.23452	6.24764	0.7046	0.3475
R01-3	3000	6002-9001	1000	9002-10001	4.12608	245.92226	0.7083	-1045.1004
R01-4	3000	8790-11789	1000	7002-8001	3.99532	36.48907	0.7126	-20.0941
R01-5	5000	2-5001	1666	9002-10667	4.06957	45.97084	0.7150	-37.0779
R01-6	5000	5002-10001	1666	2002-3667	4.05875	458.26447	0.7170	-3622.5493
R01-7	8000	2-8001	2666	8002-10667	4.10478	3.89606	0.7131	0.7231
R01-8	8000	3790-11789	2666	2-2667	4.05925	3.97338	0.7155	0.7200

R² Regression analysis represents the best results when: (i) a square multiple regression coefficient is close to 1 and (ii) the root mean square error (RMSE) reaches the zero value. The square multiple regression coefficients R² and the root mean square error (RMSE) are given by

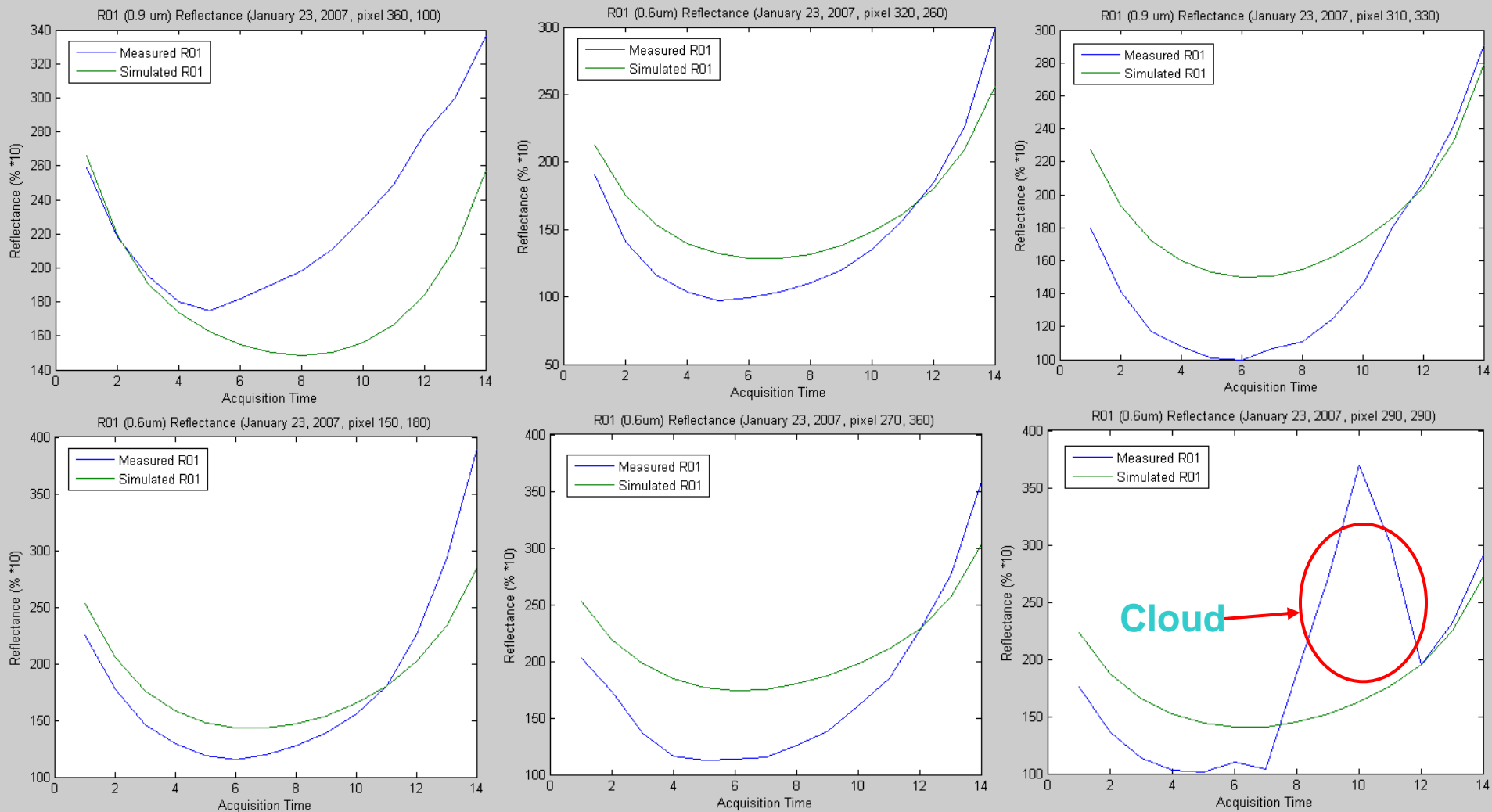
$$R^2 = 1 - [\sum (y_j - y_{j,\text{comp}})^2 / \sum (y_j - y_{\text{mean}})^2]$$

$$\text{RMSE} = \sqrt{S^2} = \sqrt{\text{SSR} / (\text{N}-\text{p})} = \sqrt{\sum (y_j - y_{j,\text{comp}})^2 / (\text{N} - \text{p})}$$

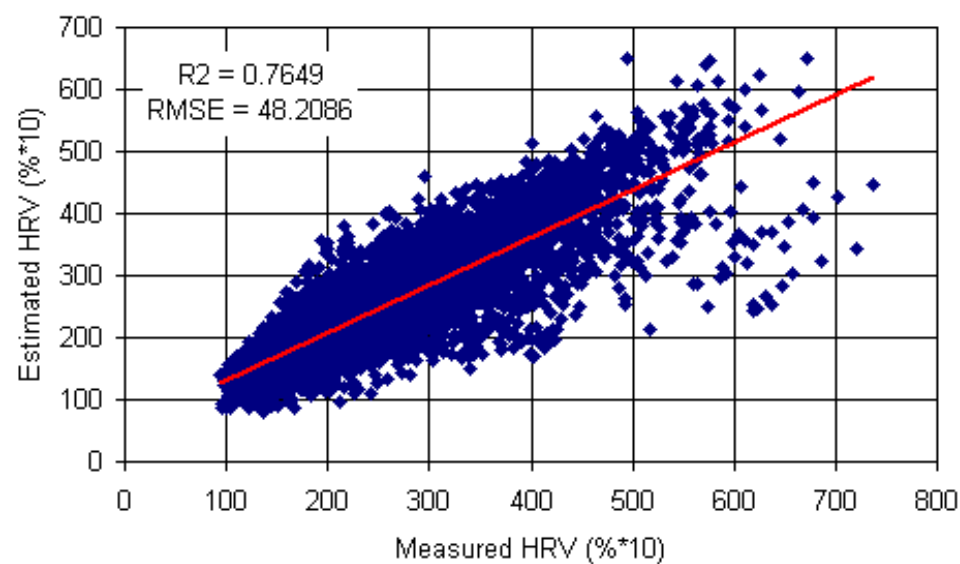
Observed (Bottom) and simulated (Up) R01 Reflectance ($0.6\mu\text{m}$), January 23



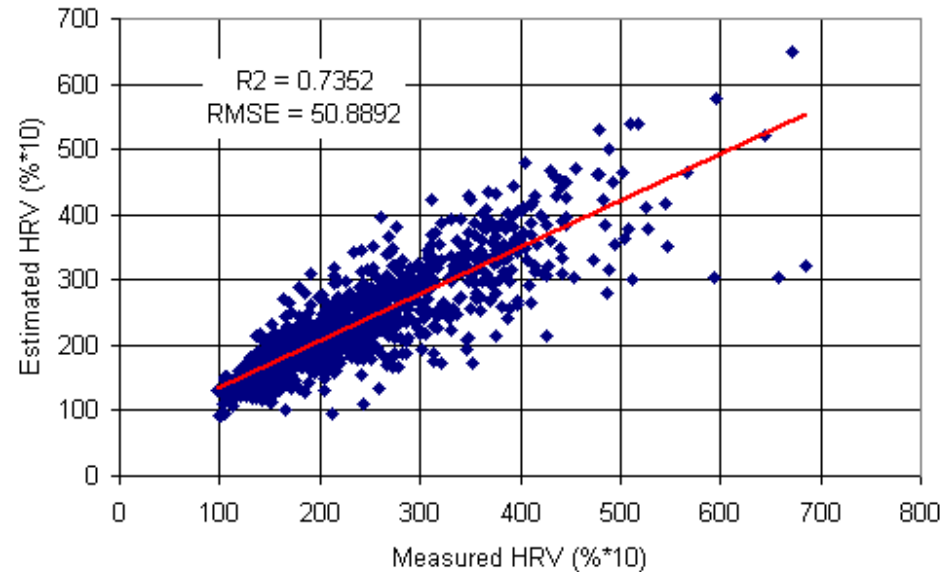
Observed vs. simulated 0.6 channel reflectance for selected pixels on January 23, 2007



Simulated vs. Observed Reflection values in Training and Validation

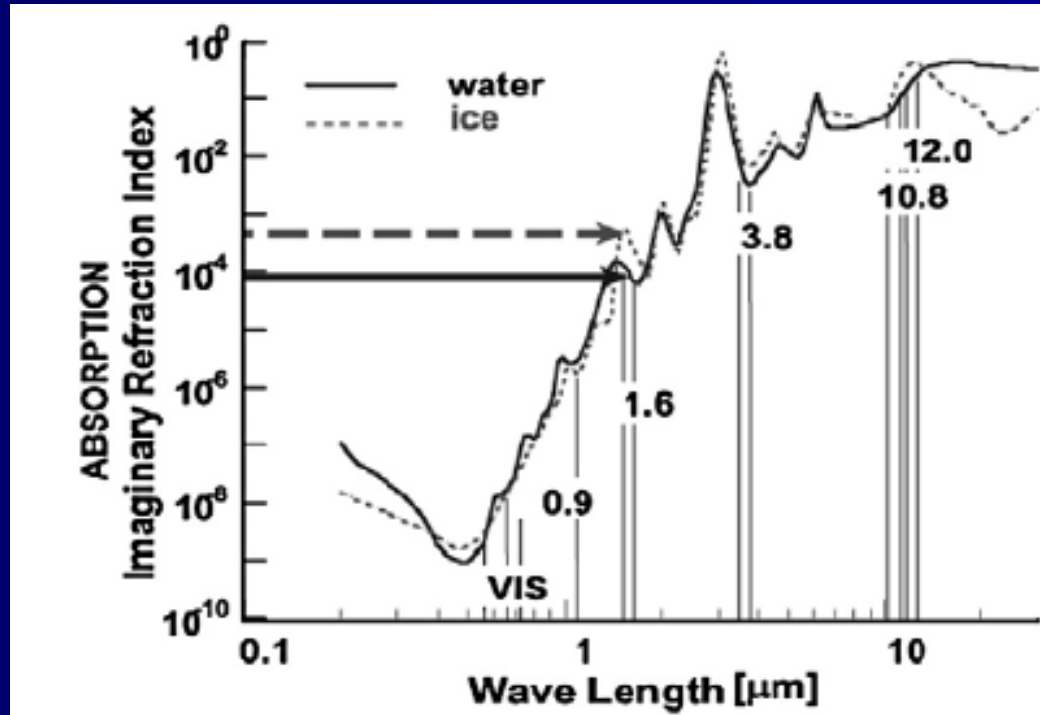


HRV-1 model, Training results



HRV-1 model, Validation results

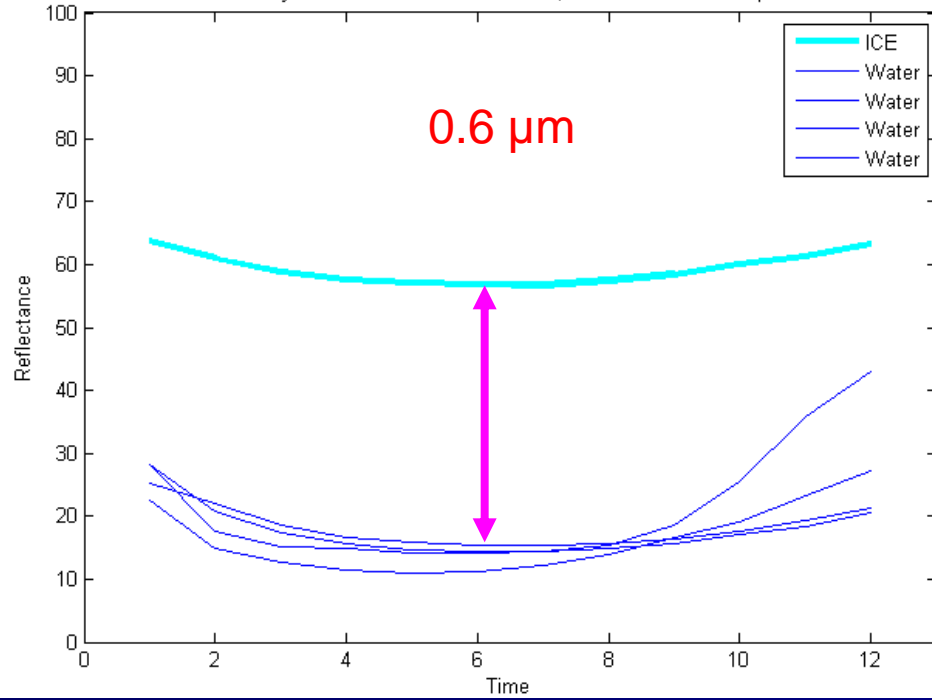
Absorption of ice (dashed) and water (solid) in different spectral regions



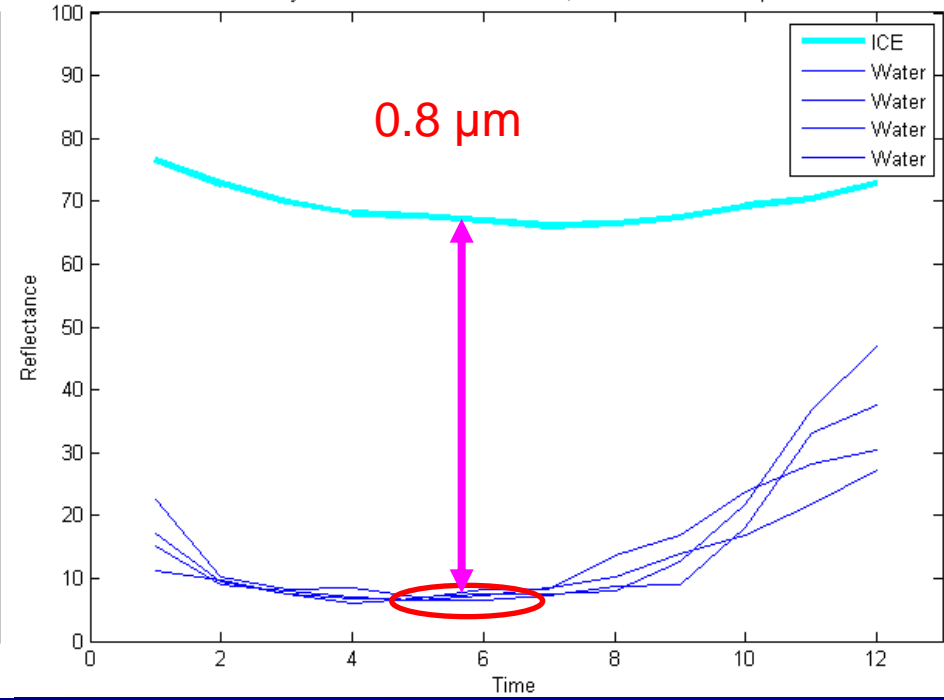
Different absorption of ice and water clouds for 1.6 μm channel is marked by arrows.

Ice and Water Hourly Variations in Visible Channels $0.6\mu\text{m}$ and $0.8\mu\text{m}$

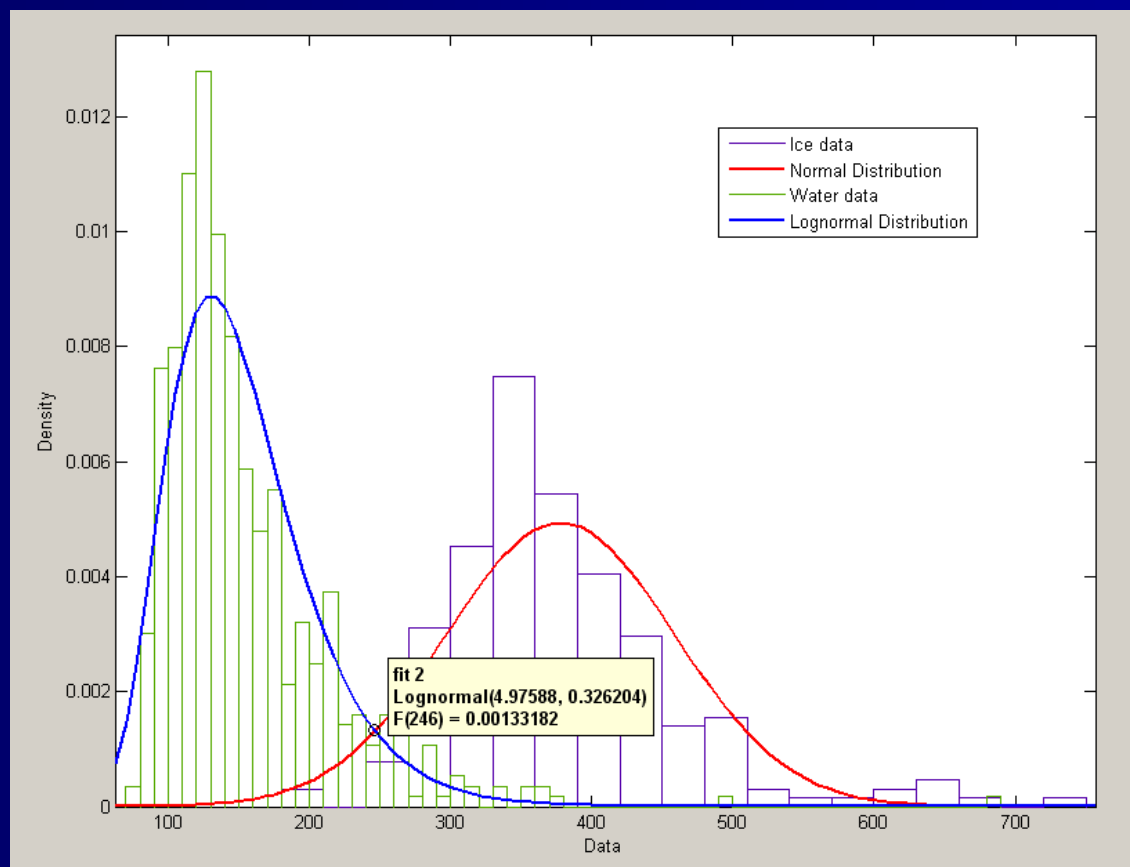
Hourly variation of reflectance for ice, water in Channel $0.6\mu\text{m}$



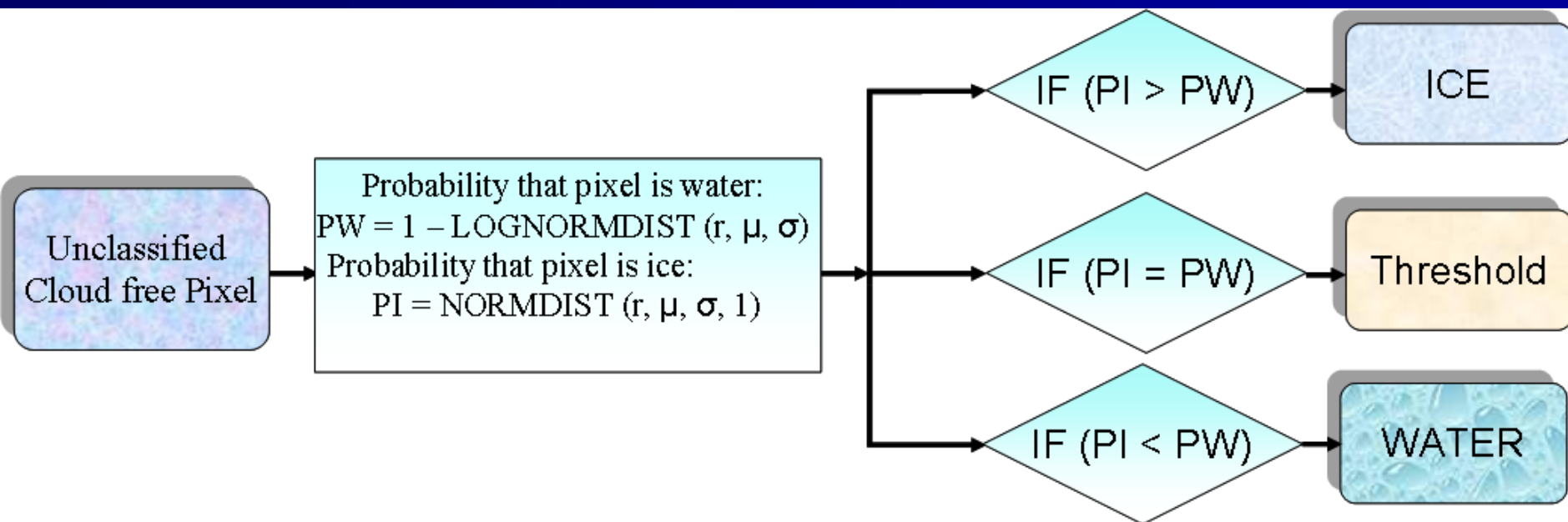
Hourly variation of reflectance for ice, water in Channel $0.8\mu\text{m}$



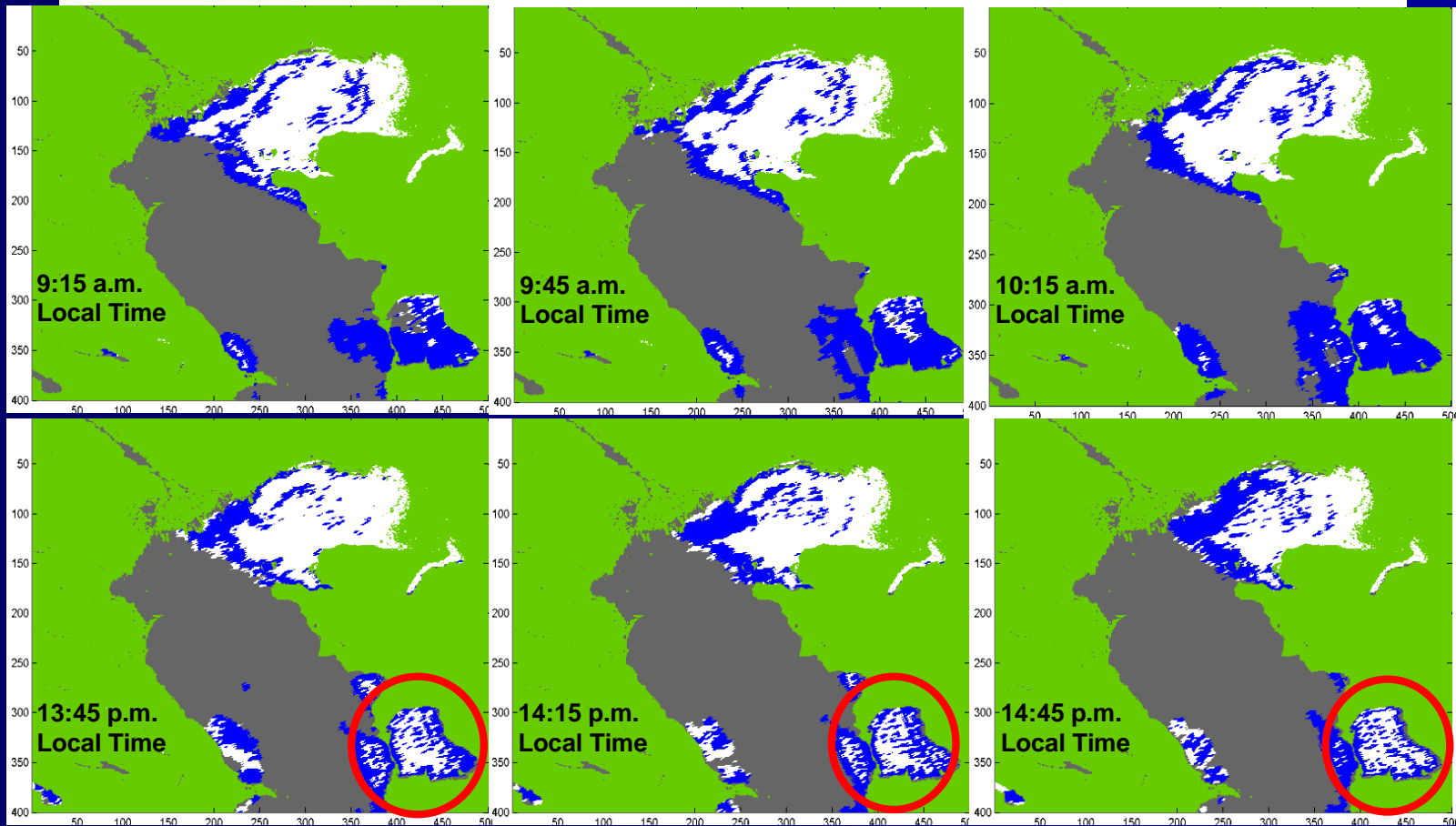
Distribution functions of water (left) and ice (right) reflectance for Feb 28, 2009



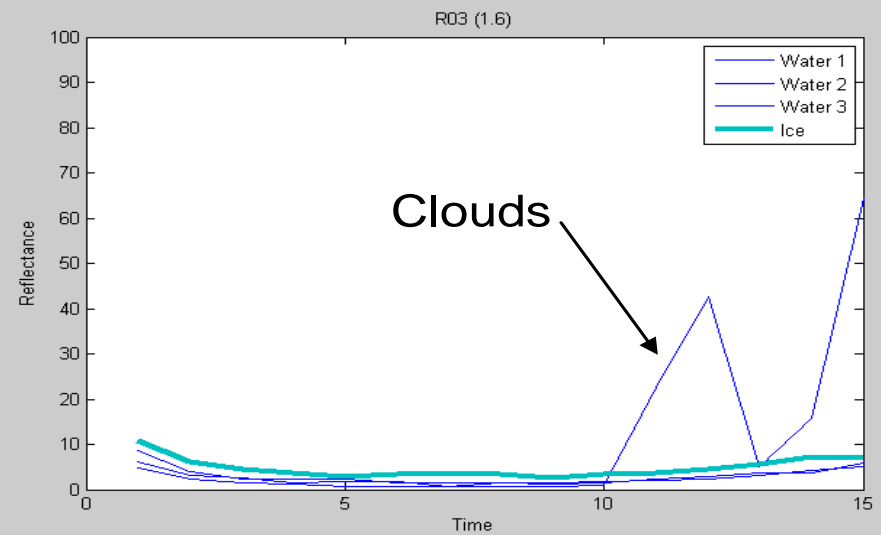
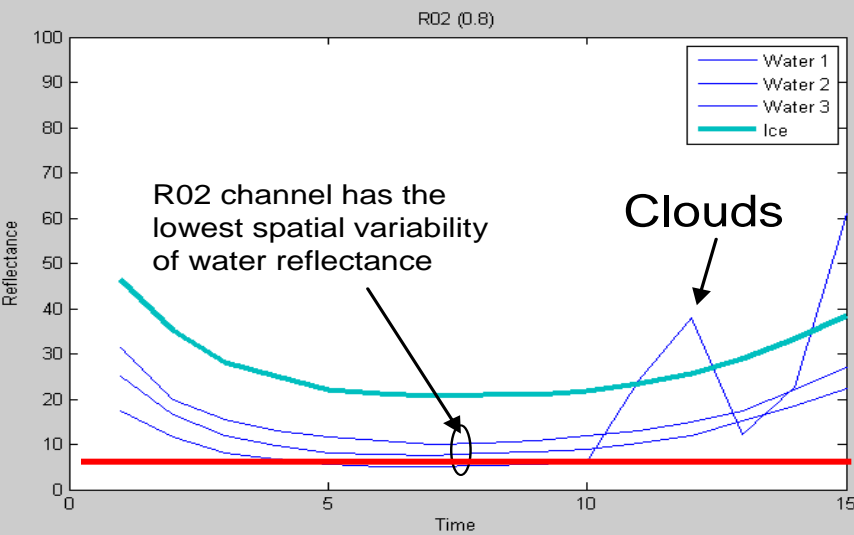
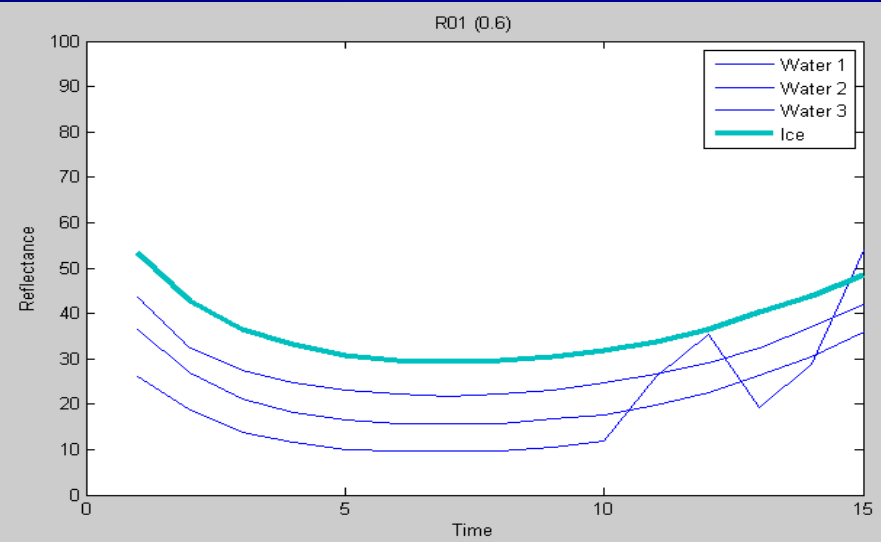
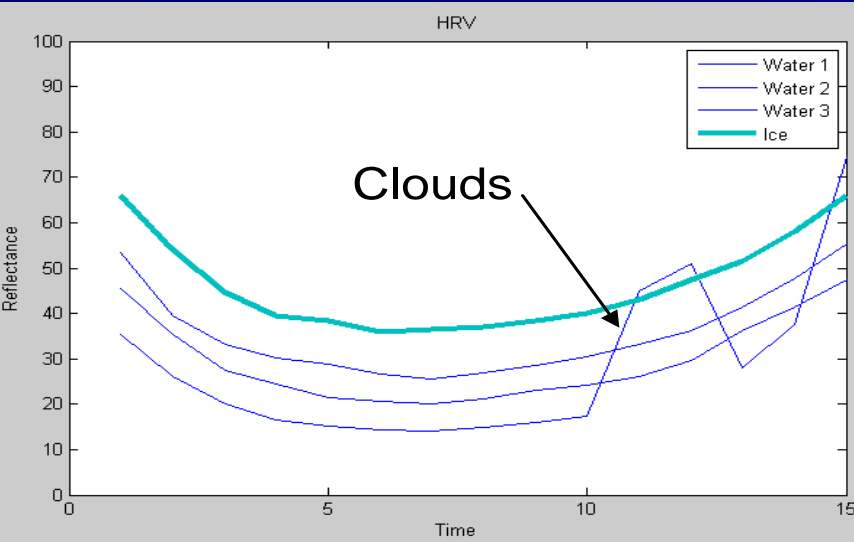
Flow Chart of the Operation for the Threshold Calculation



Classified images with **Constant Daily threshold**, Caspian Sea mid winter, Feb 28, 2007



Hourly variation of reflectance for one Ice and three water pixels in the visible channels



Bidirectional Reflectance Distribution Function (BRDF)

Adaptation of existing bidirectional reflectance distribution function model (BRDF) to reduce errors introduced by the viewing geometry effects. Using kernel-driven approach. Two different models will be adapted and evaluated: Walthall and Roujean *et al.*

General BRDF Model:

$$\rho(\theta_s, \theta_v, \varphi)$$

$$= R_0 \left[1 + \left(\beta_0 + \beta_1 \sin\left(\frac{\varphi}{2}\right) + \frac{\beta_2}{\cos\theta_s} \right) \sin\theta_v \right] \quad (\text{A4})$$

+ water-related parameter

where ρ =reflectance factor; θ_s =solar zenith angle; θ_v =view angle; φ =relative azimuth; R_0 =nadir reflectance factor; β_0 , β_1 , β_2 =empirical parameters.

Differential Angles

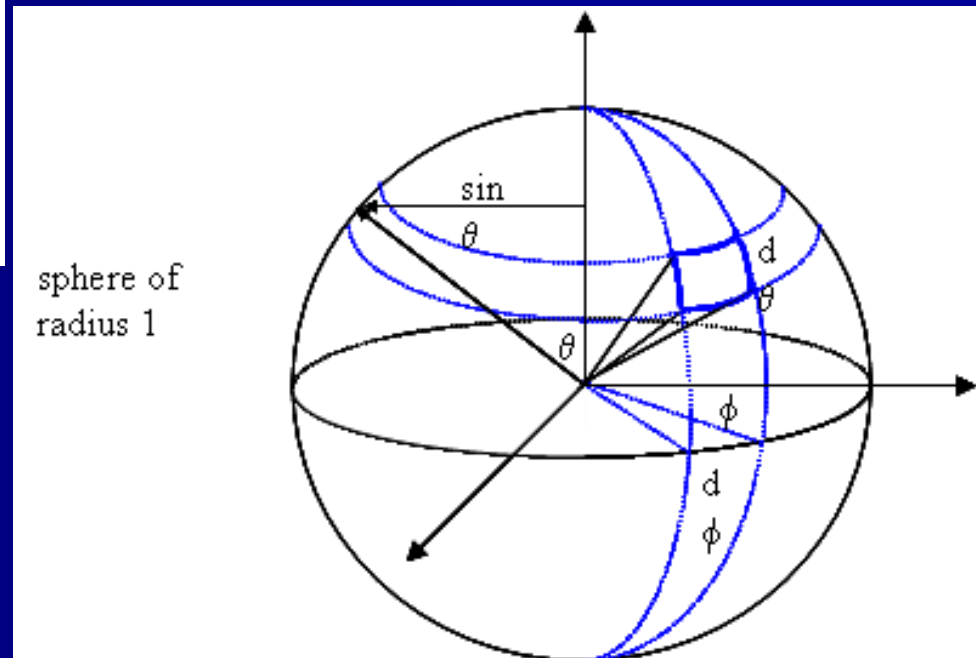
- The differential solid angle is defined to be the area of the small blue patch
- Given spherical coordinates (θ, ϕ) and small differential angular changes denoted $d\theta$, $d\phi$, the differential solid angle, $d\omega$, is defined to be:

$$d\omega = (\text{height})(\text{width})$$

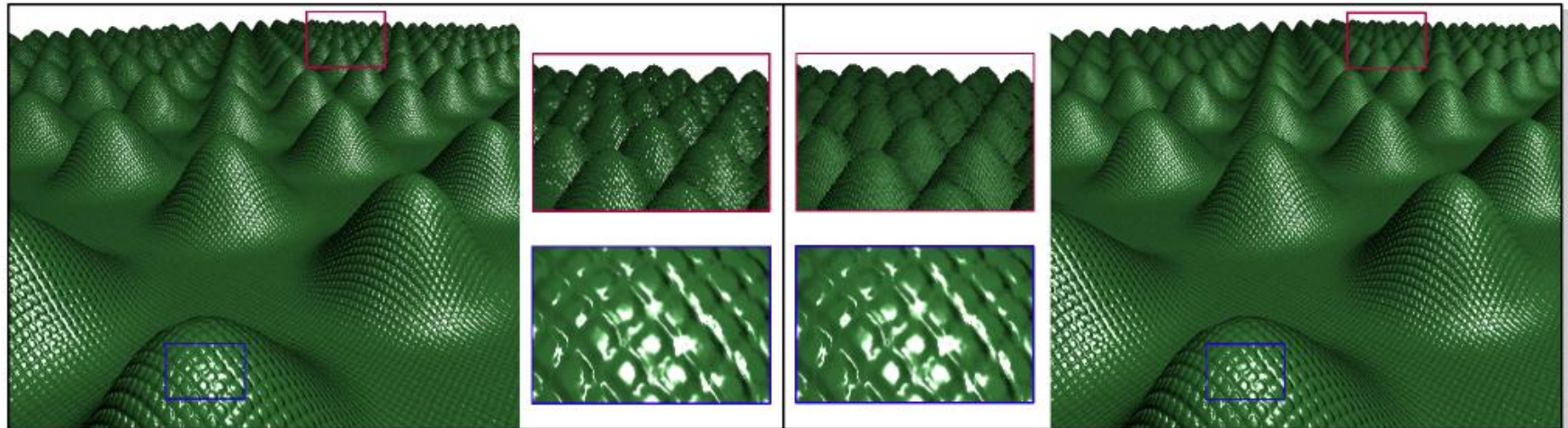
$$d\omega = (d\theta)(\sin \theta d\phi)$$

$$d\omega = \sin \theta d\theta d\phi$$

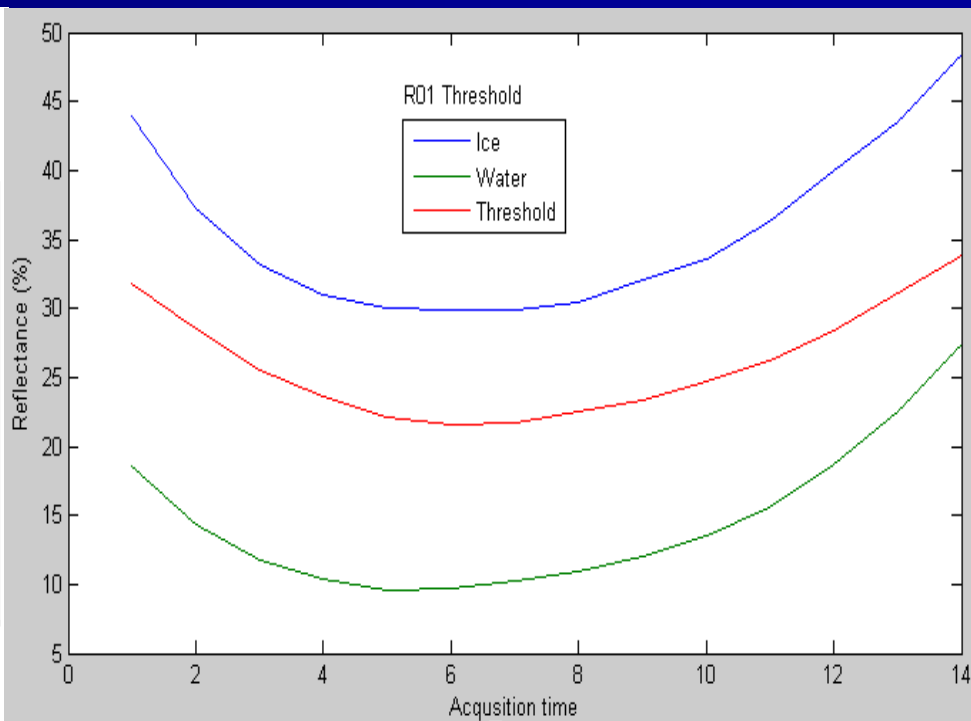
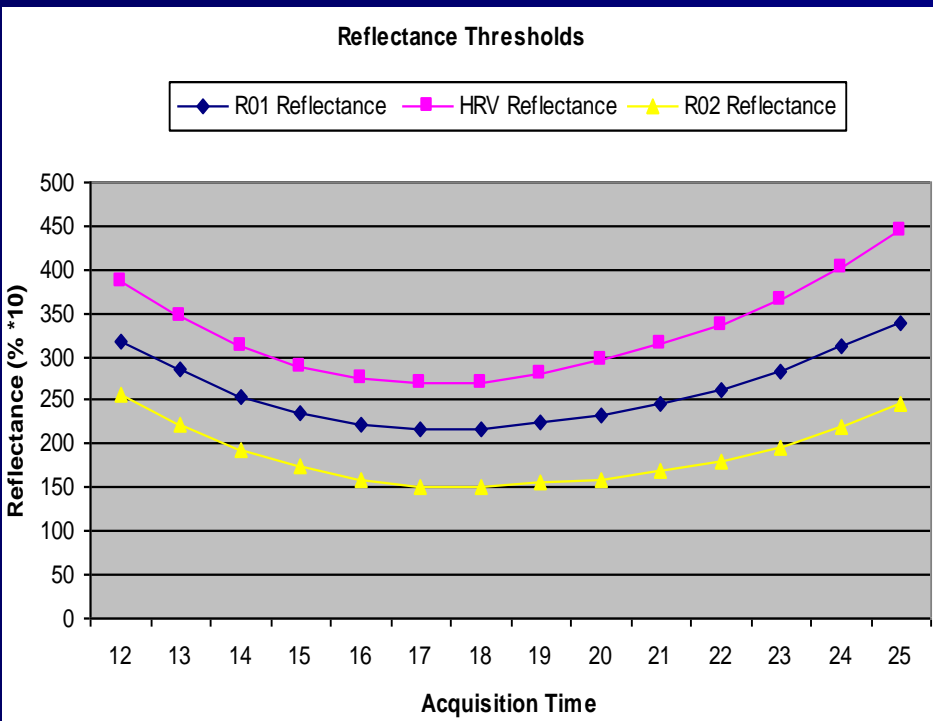
- The area quantity has units of radians squared, or steradians



Sample images of kitchen sponge texture with viewpoint variation, top, and lighting direction variation, bottom. Each image has been recited to a frontal view.

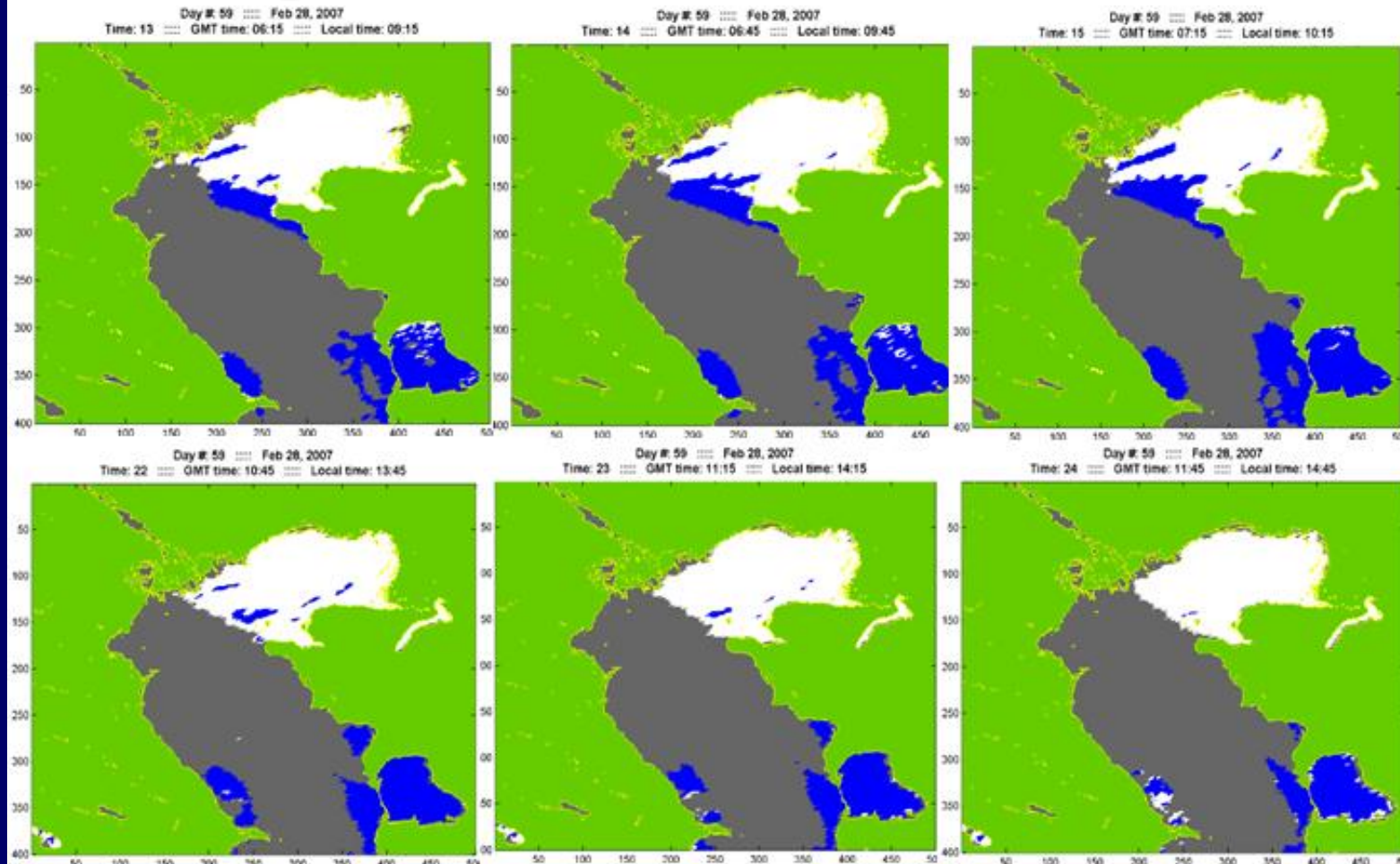


Threshold values for HRV, R01 and R02 Reflectance during local acquisition time 8:45 to 15:15



The dynamic threshold (Red) in R01 (0.6 μ m) classifying Ice and Water Pixels (Right)

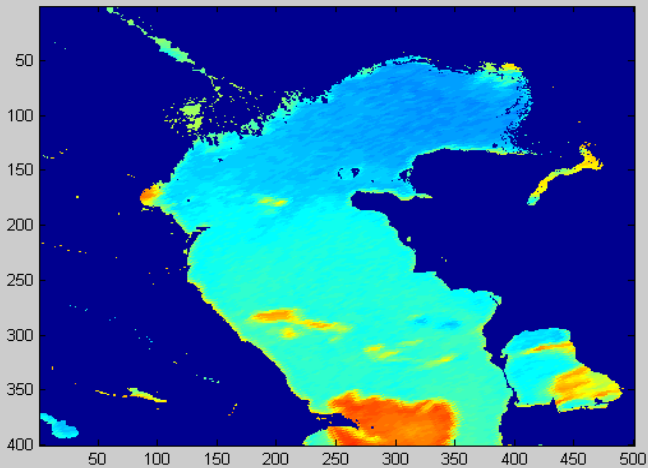
Classified images with Dynamic threshold, Caspian Sea mid winter, Feb 28, 2007



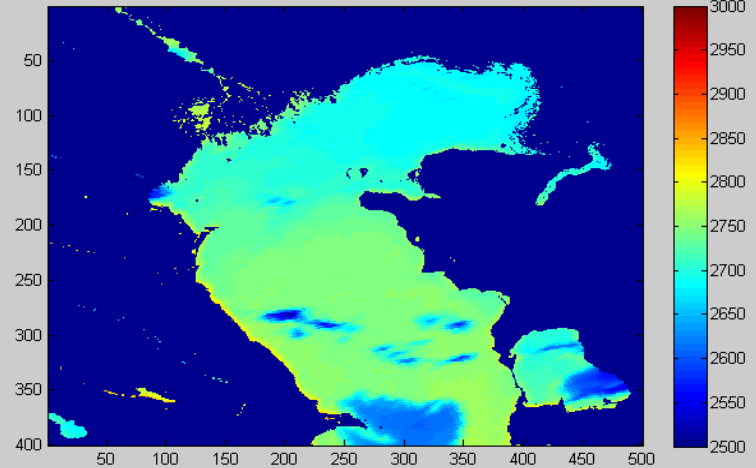
January 23, 2007 11:45 local time

Temperature Channels

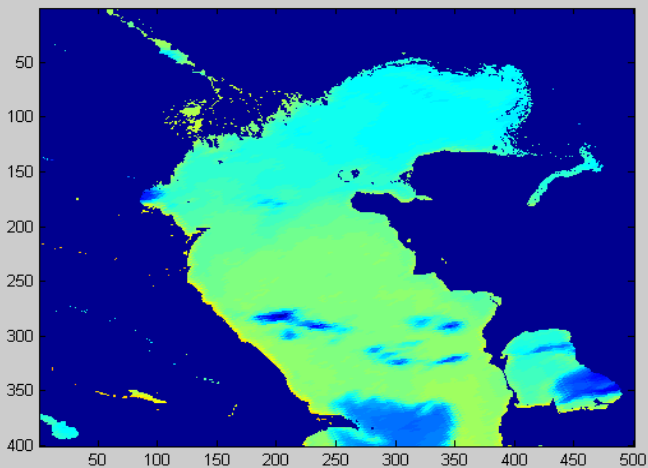
T04: IR 10.8 IR Window Channels



T09: IR 12.0 IR Window Channels



T10: IR 13.4 CO2 Channel

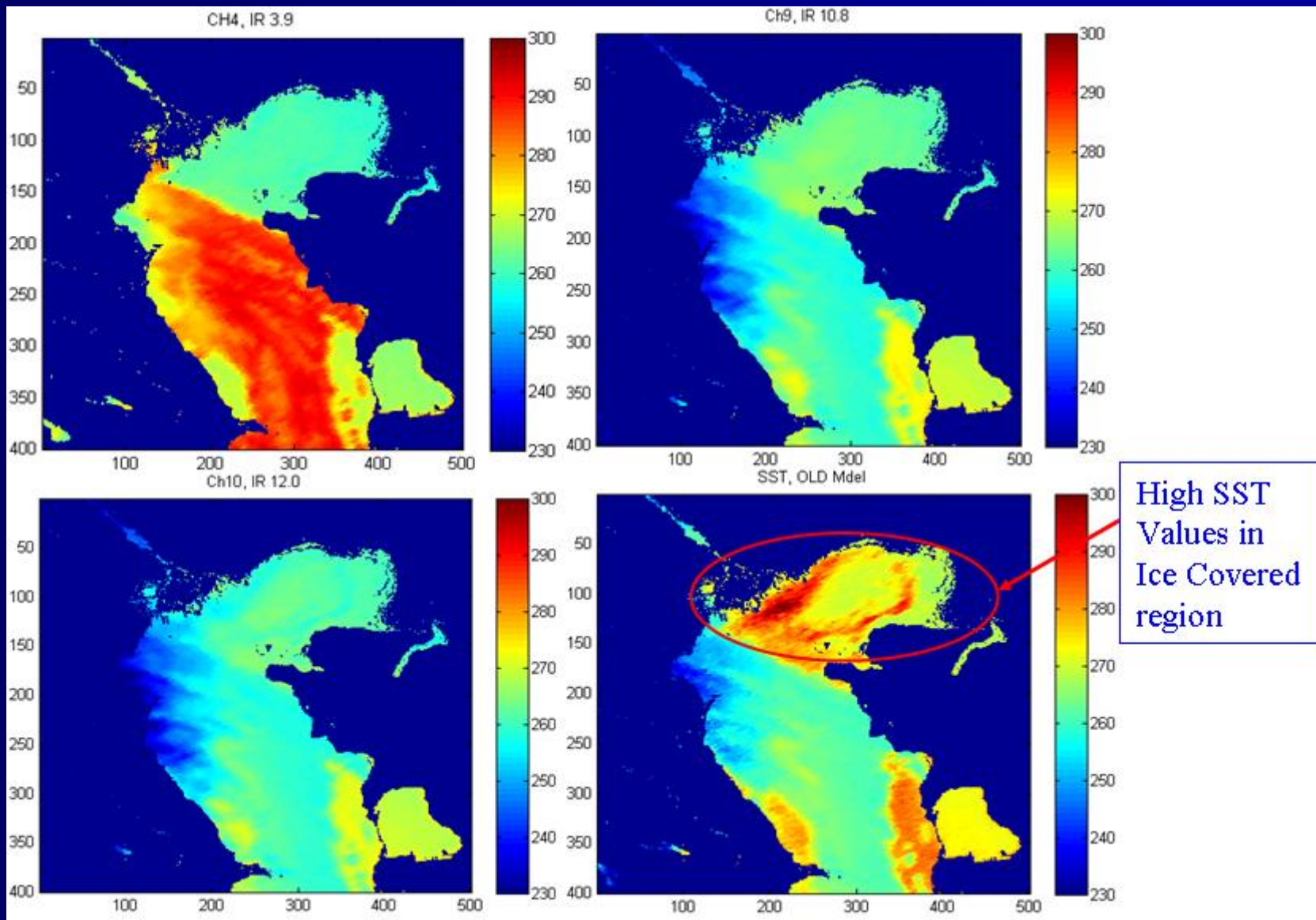


Sobrino and Romaguera's Suggested SST Algorithm

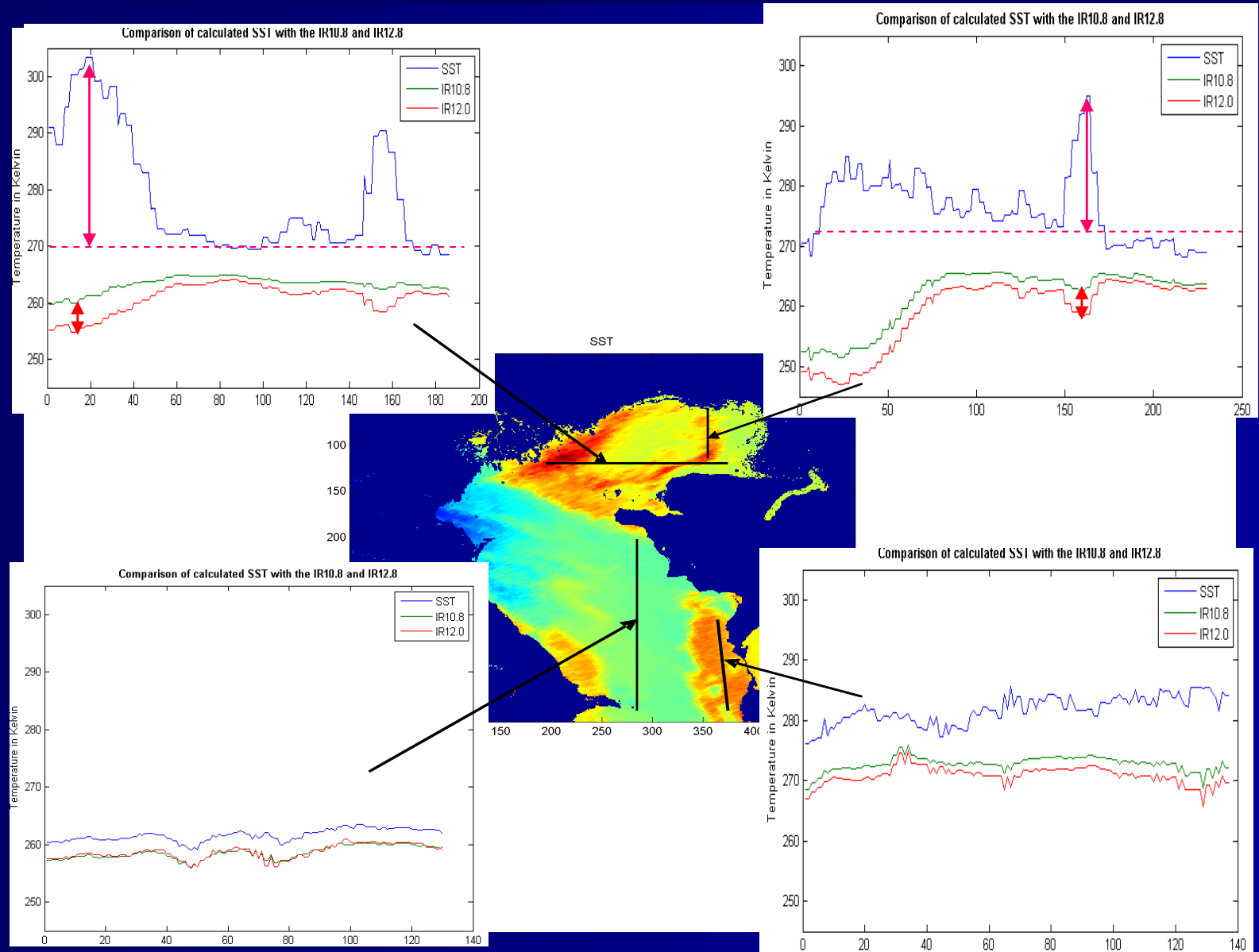
$$SST = T_{IR10.8} + [0.99\cos\theta + 0.21\theta] * (T_{IR10.8} - T_{IR12.0}) +$$

$$[(0.364/\cos\theta) + 0.15] * (T_{IR10.8} - T_{IR12.0})^2 + [(0.327/\cos^2\theta) + 0.11]$$

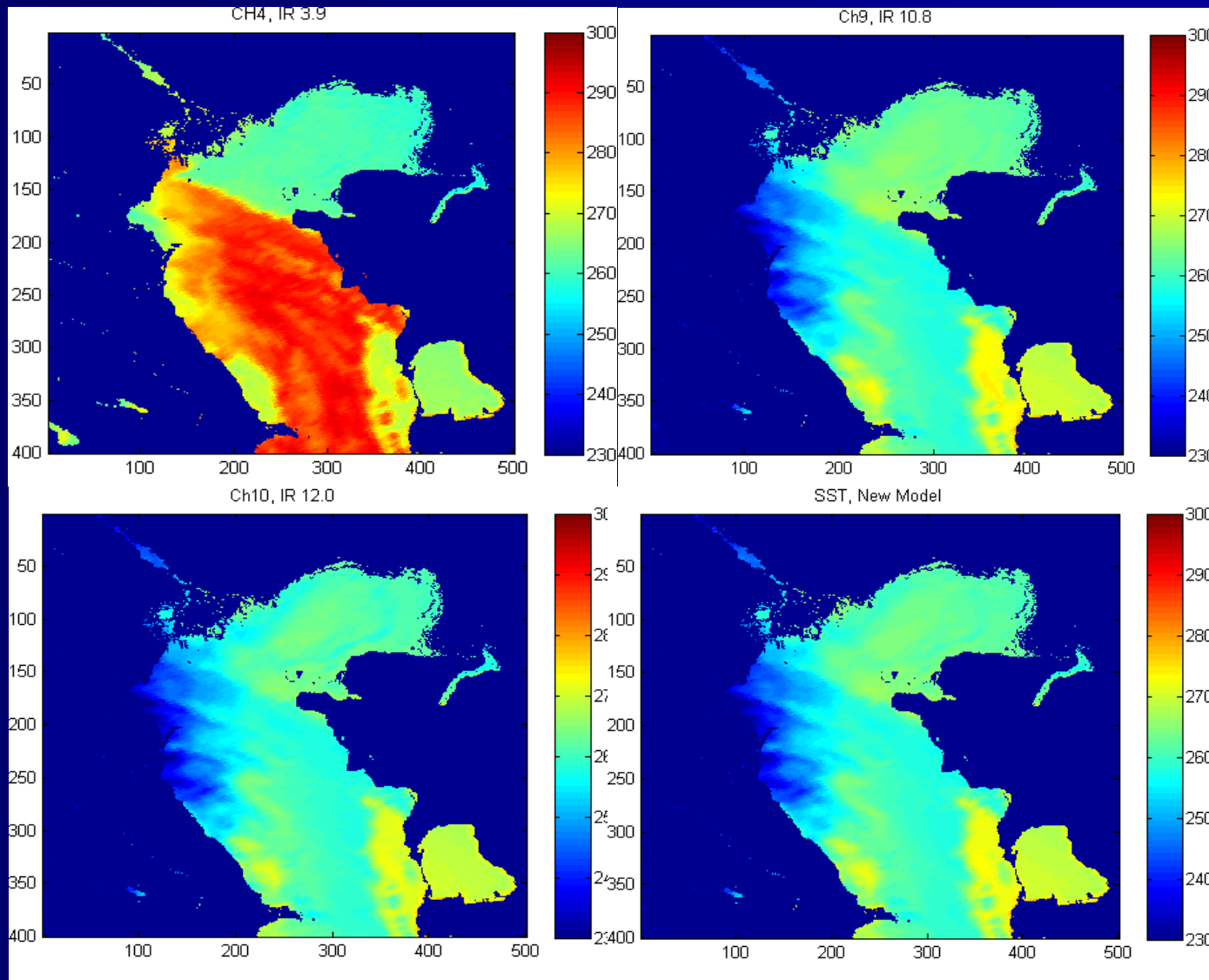
Temperature Channels and the existing SST Model



Transect of temperature in various regions for comparison of calculated SST with the IR10.8 and 12.0



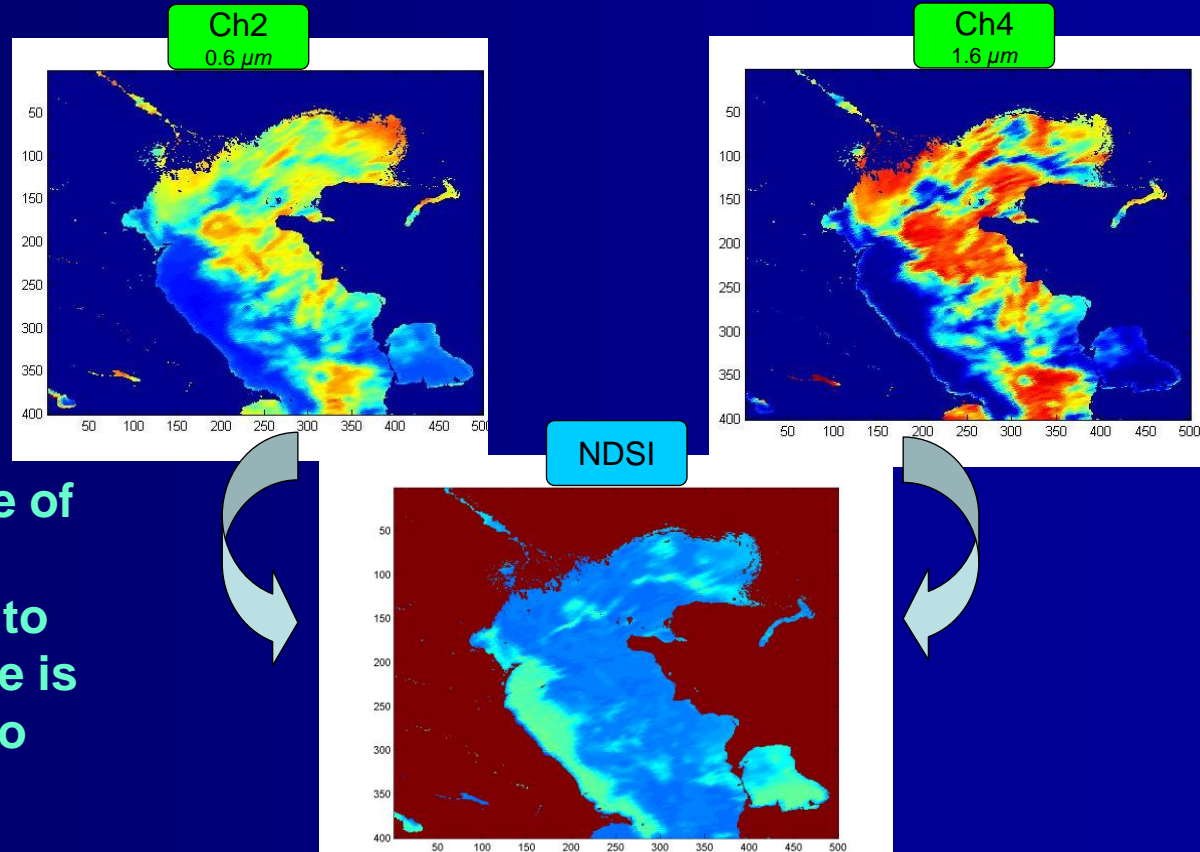
New SST Model (bottom right) shows consistent ice presence for data taken during winter of 2007 of the Caspian Sea



Normalized Difference Sea Ice Index (NDSI)

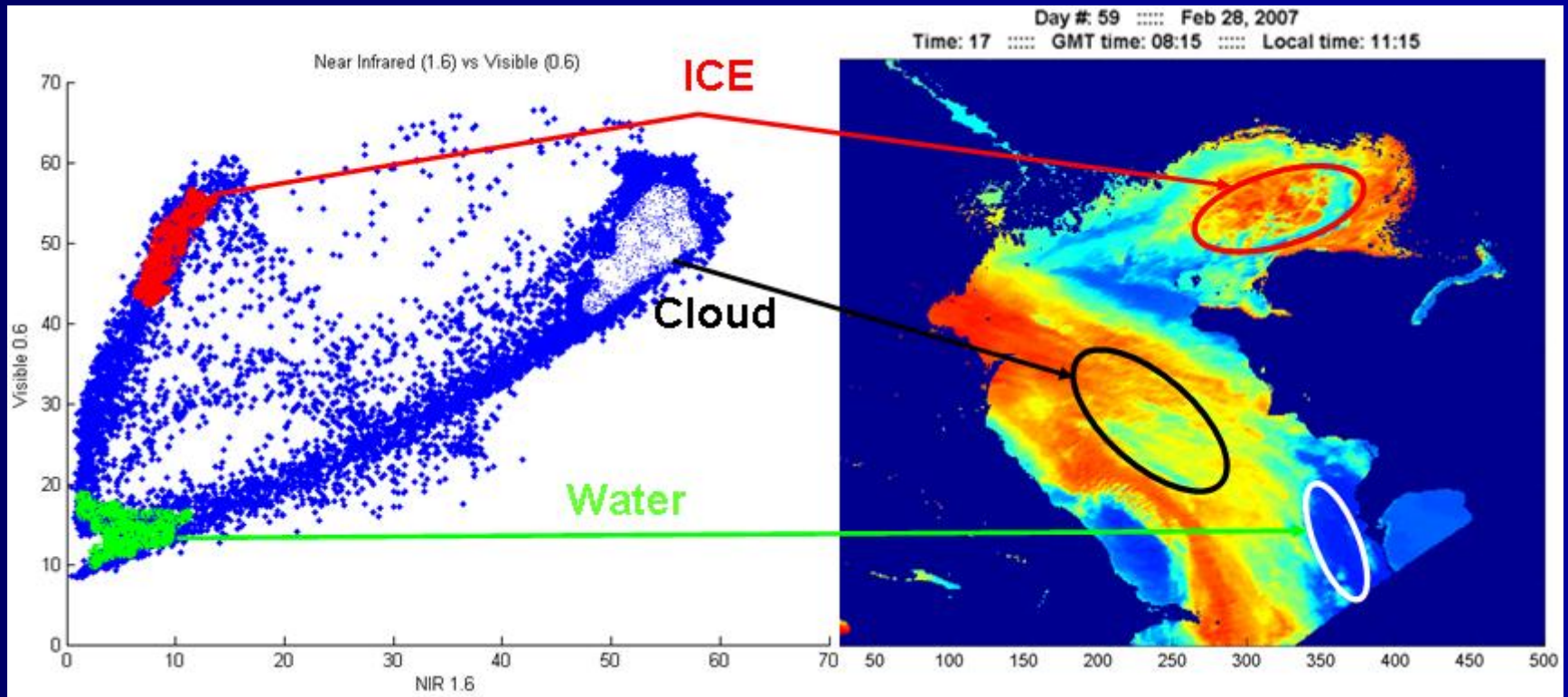
The Normalized Difference Sea Ice Index (NDSI) in simple wording is a numerical indicator or index value that analyzes remote sensing measurements such as reflection values in order to assess the existence of sea ice in a given pixel. Thus, sea ice in mixed pixels has an NDSI that is less than what normally is for pure Sea Ice. METOSAT-8 bands 2 (0.6 μm) and 4 (1.6 μm) have been used to calculate the NDSI.

$$\text{NDSI} = (\text{band 2} - \text{band 4}) / (\text{band 2} + \text{band 4})$$



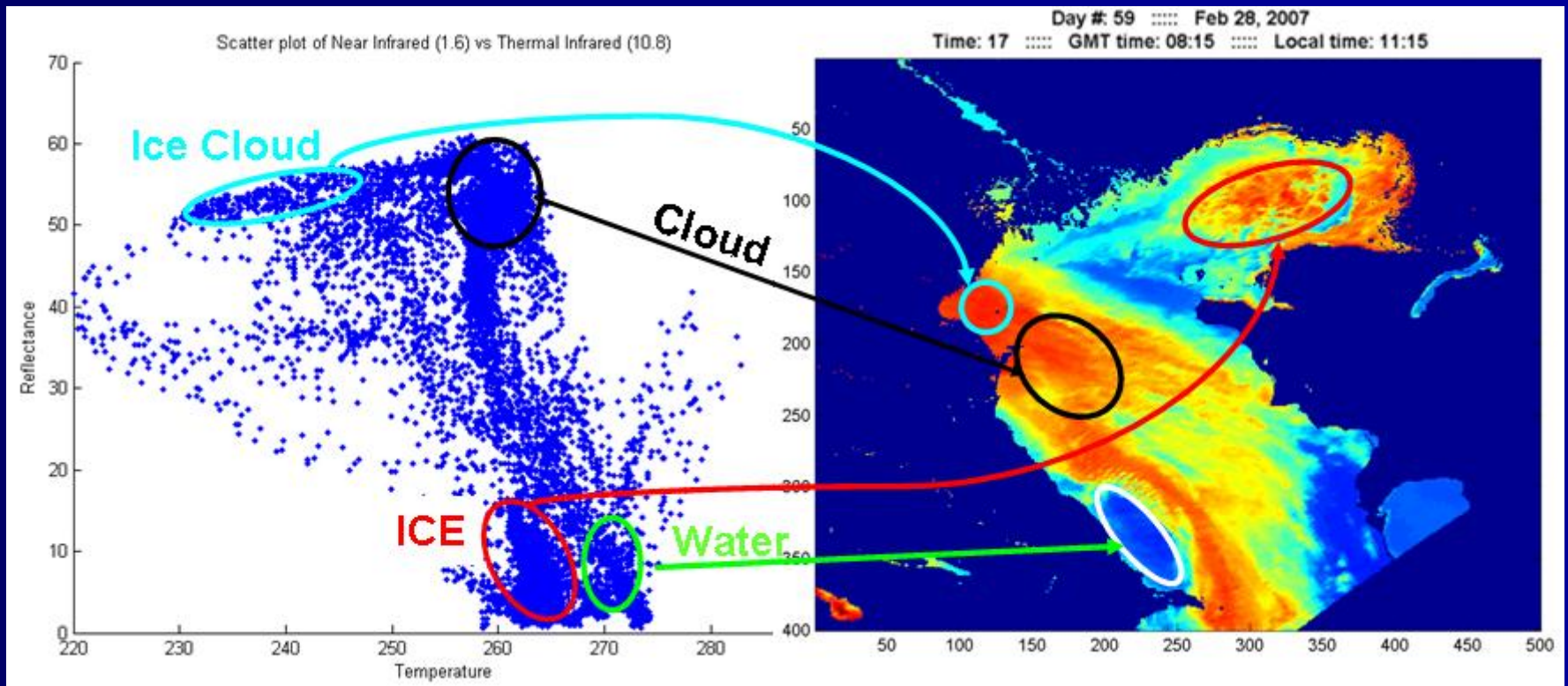
Pure sea ice can be distinguished by its high NDSI value. One of the classification threshold for a pixel to be mapped as sea ice is that the NDSI value to be 0.4 or more.

Channels Correlation Analysis



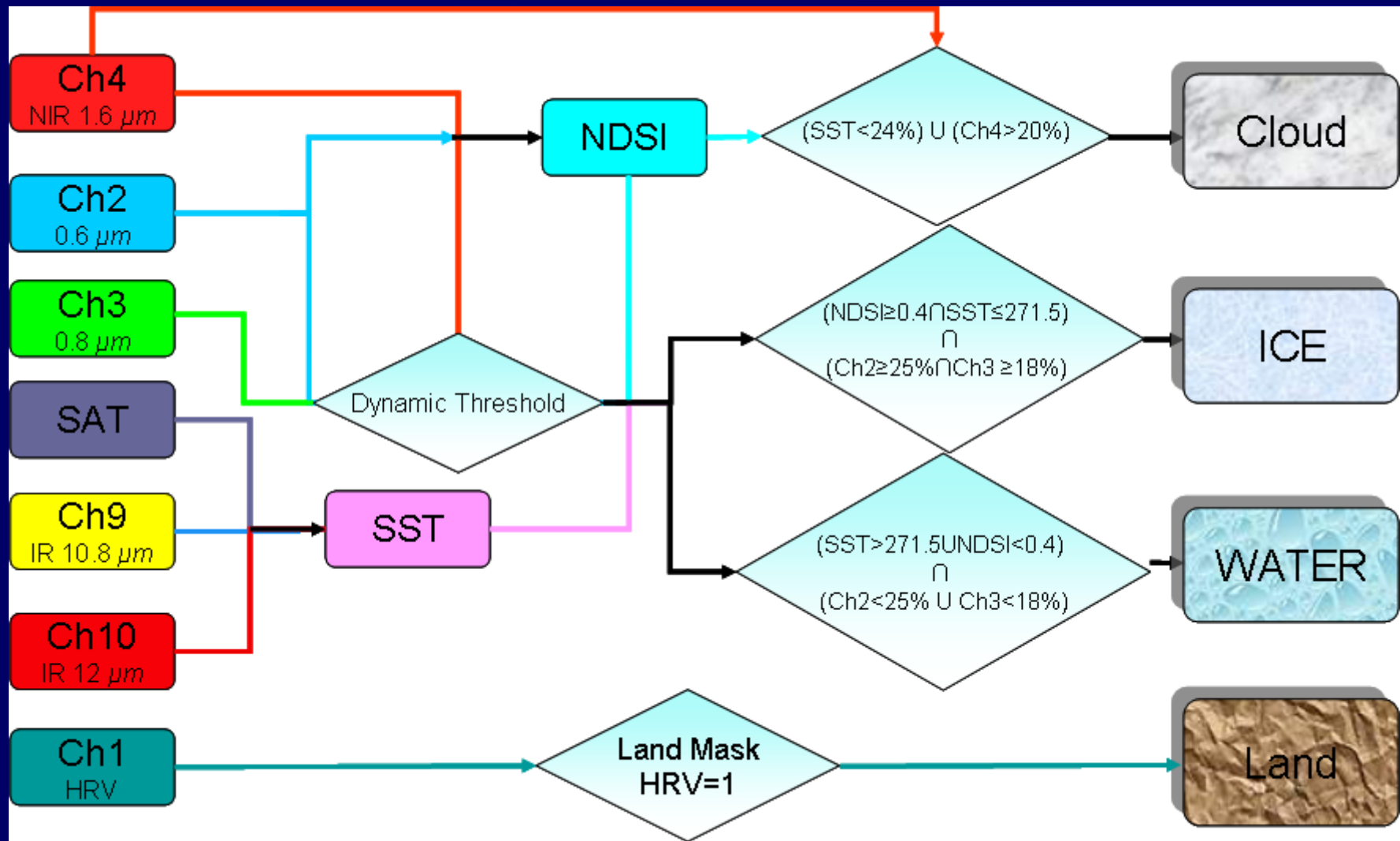
Scatter Plot (left) of near infrared (band 1.6) vs. visible (0.8), HRV image (right) shows clouds (black oval), Ice (red oval) and Water (white oval)

Channels Correlation Analysis Cont.



Scatter Plot (left) of near infrared (band 1.6) vs. thermal infrared (band 10.8) HRV image (right) shows clouds (black oval), ice cloud (blue), Ice (red oval) and Water (white oval)

Flow Chart of the Operation for Sea Ice Mapping



Spectral based sea ice mapping model

Classification Process

Land = Green



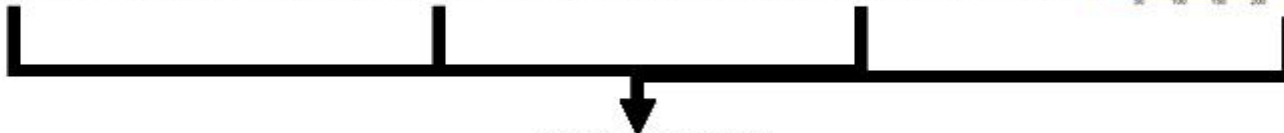
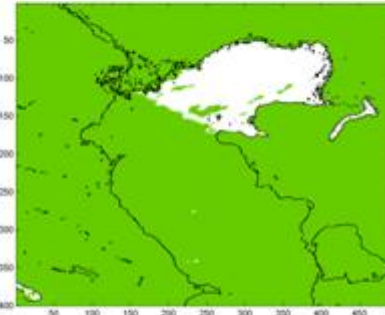
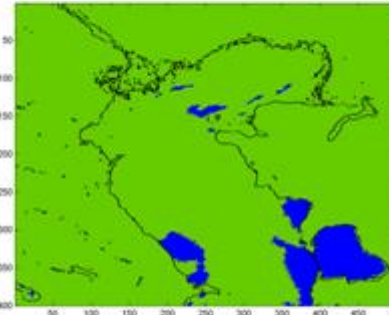
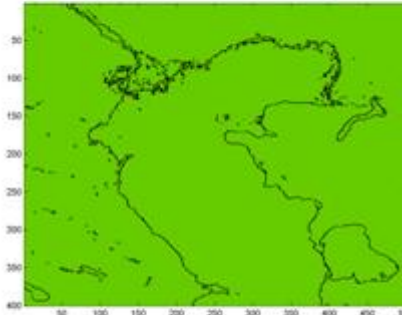
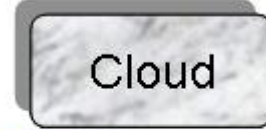
Water = Blue



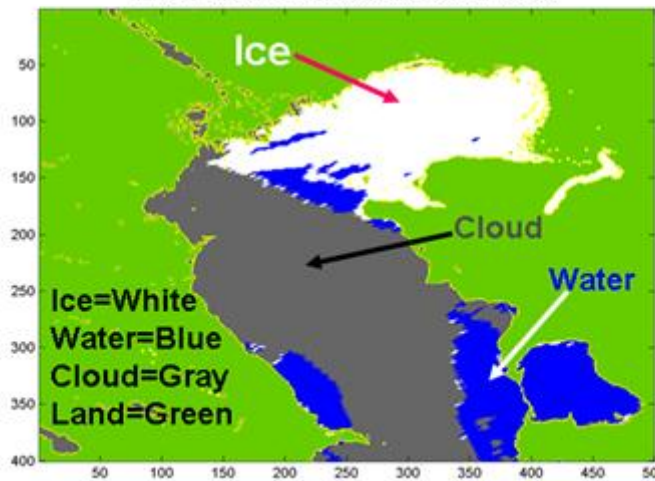
Ice = White



Cloud = Gray



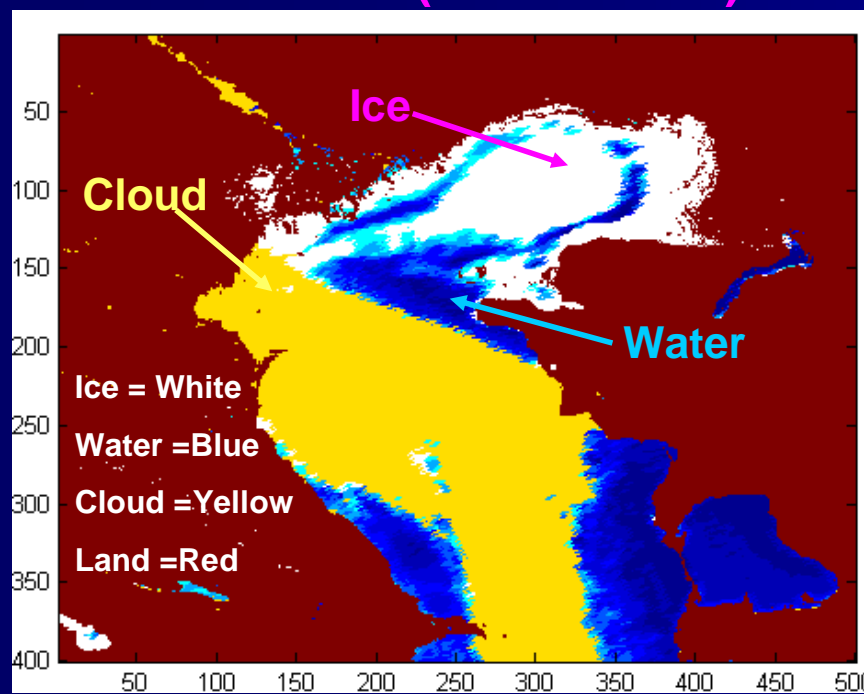
Day #: 59 Feb 28, 2007
Time: 17 GMT time: 08:15 Local time: 11:15



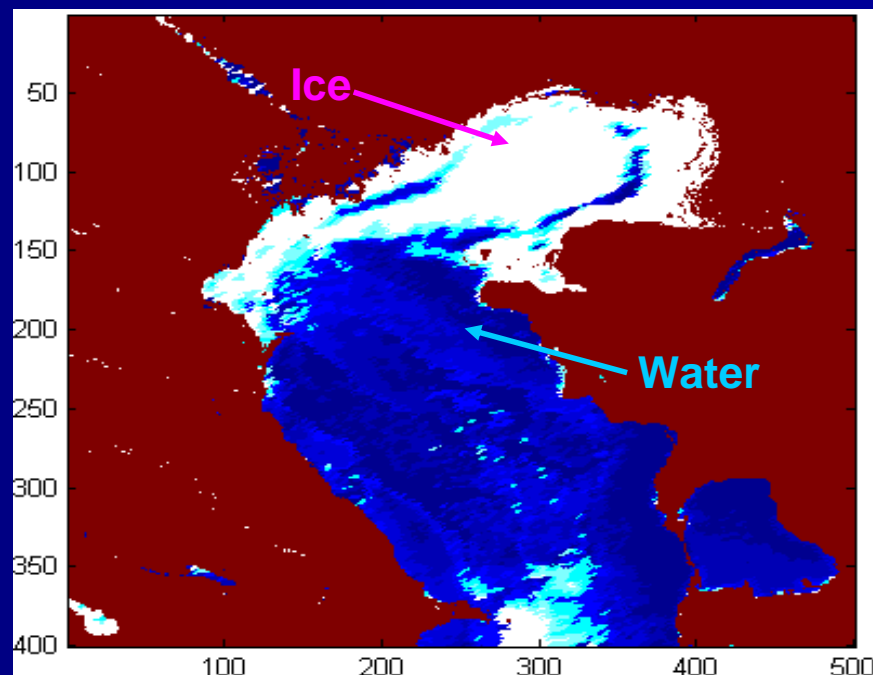
Daily and Multi day composited Ice Maps

February 28th, 2007

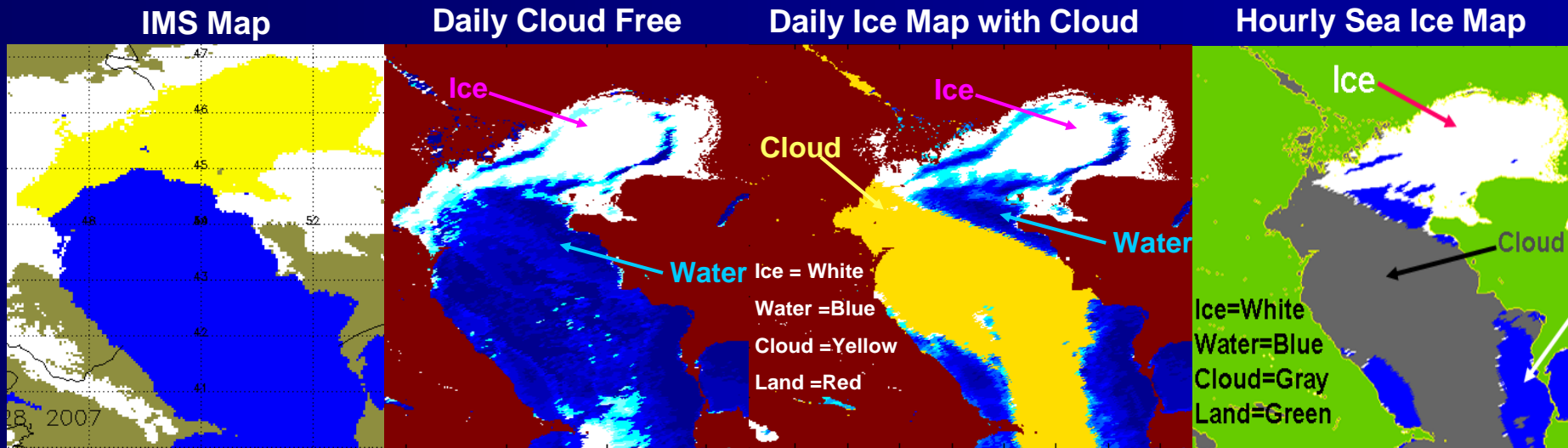
Product 1 (with clouds)



Product 2 (cloud free)



Model Comparison



IMS Map and models generated sea ice maps of February 28th, 2007 of Caspian Sea

Conclusion

- The rate of observations from SEVIRI (one image per 15 minutes) is the same as for GOES-R ABI. The developed ice detection and mapping algorithm have been applied to MSG SEVIRI data and have been tested over the Caspian Sea.
- SEVIRI is missing several spectral channels, which are not critical for the ice mapping and will be available in ABI.
- The temperature difference between the water and the land surface creates a convective condition over the Caspian Sea which generates a frequent and thick cloud coverage, Consequently, it is almost impossible to have a clear sky condition over the Caspian Sea for all pixels during a winter day, which makes the production of timely classification of the ice coverage and reducing the temporal resolution of the final product difficult .
- Processing all reflectance pixels collected over the Caspian Sea between December 2006 and February 2007, the average time between two clear sky conditions is 2.85 days. However, the use of night brightness temperature has reduced the time gap to 2.25 days and decreased the number of unclassified pixels (cloudy pixels) by 10 to 30% for most days.

Suggested Future work

- Develop a technique to derive ice fraction and concentration which improves classification and makes it possible to add fractional and shallow ice as additional class to the final product.
- Testing and validating the developed technique for winter 2007-2008 for Caspian sea, over seas and large lakes in Europe that are getting seasonal ice cover (Gulf of Bothnia, Gulf of Finland).
- Prepare technical documentation for all developed algorithms.
- Prepare the developed software for operational implementation at NESDIS

Acknowledgment

This study was supported and monitored by National Oceanic and Atmospheric Administration (NOAA) under Grant NA06OAR4810162. The views, opinions, and findings contained in this report are those of the author (s) and should not be construed as an official National Oceanic and Atmospheric Administration or U.S. Government position, policy, or decision.

- Rouzbek Nazari and Reza Khanbilvardi, Application of Dynamic Threshold in Development of an Advanced Technique for Mapping and Monitoring Sea and Lake Ice, Working Paper
- ROUZBEH NAZARI, VANESSA CLARK and REZA KHANBILVARDI, Assessment of Sea Surface Temperature (SST) and Normalized Difference Sea Ice Index (NDSI) Derived from MSG SEVIRI Satellite for Sea Ice Applications, International Journal of Remote Sensing, Submitted on 29-Nov-2009
- Rouzbek Nazari, Magdalena Rychtecka, Hosni Ghedira and Reza Khanbilvardi, Stepwise Linear Regression for mapping and monitoring sea and lake ice for the future GOES-R, International Journal of Terraspace Science and Engineering , Volumn I, Issue 2, June, 2009
- R. Nazari, NOAA-CREST, New York, NY; and Hosni Ghedira, M. Temimi, P. Romanov, and R. Khanbilvardi Development and validation of a BRDF model for ice mapping for the future GOES-R Advanced Baseline Imager (ABI) using Artificial Neural Network, The 88th Annual Meeting (20-24 January 2008) (New Orleans, LA)
- Rouzbek Nazari, Marouane Temimi, Hosni Ghedira and Reza Khanbilvardi, NOAA- CREST New York City, New York, An automated approach for sea ice mapping and ice fraction determination for the
- future GOES-R Advanced Baseline Imager (ABI), 2008 IEEE International Geoscience & Remote Sensing Symposium, July 6-11, 2008, Boston, Massachusetts, U.S.A
- R. Nazari, S. Mahani, and R. Khanbilvardi, Climate Changes Interaction with Tropical Storm (Hurricane), Fourth Annual NOAA-CREST Symposium, February 23-25 2006, Puerto Rico, Mayaguez
- R. Nazari, S. Mahani, and R. Khanbilvardi, Changes in Sea Surface Temperature and North Atlantic Hurricane Activities, AGU Joint Assembly, May 23-25 2006, Baltimore, Maryland
- R. Nazari, S. Mahani, and R. Khanbilvardi, Impacts of Climate Change and Tropical Storms (Hurricanes) on Coastal regions, 27th Conference on Hurricanes and Tropical Meteorology, 2006, Monterey, California
- Nazari, Rouzbek and Eslamian, S. S., Management, Optimization and Simulation for an Optimum Distribution of Water in Kalamarz Multi-Reservoir System, Mianeh Basin. 6th International Conference on Hydro science and Engineering (ICHE-2004), Brisbane, Australia, May 30-June 2, 2004.
- Nazari, R., Tabatabaei H., Abedi Koupai, J., A Mathematical & Management Model of Ground Water with Emphasis on Artificial Recharge for Damaneh Plain, The Second International Conference on Salt Water Intrusion and Coastal Aquifers, Mirada, Mexico, 2003
- Nazari, R. and Eslamian, S. S. Hydrological Homogeneity Test of Catchments Using L-moments Diagram, International Conference on the Rational Use and Conservation of Water Resources in a Changing Environment, Yerevan, Armenia, 2003.